POLITECNICO
MILANO 1863

POLITECNICO DI MILANO

SCUOLA DI INGEGNERIA INDUSTRIALE E DELL'INFORMAZIONE

CORSO DI LAUREA MAGISTRALE IN INGEGNERIA FISICA

Dynamic Monte-Carlo Simulations on Anisotropic Ising Systems

Autore : Thibaud COUPÉ
Numero di matricola : 963776

Relatore : Prof. Ezio PUPPIN
Correlatore : Dr. Federico ETTORI

Anno accademico 2021-2022

Acknowledgements

Vorrei innanzitutto ringraziare il mio relatore, il Prof. Ezio PUPPIN, e il mio correlatore, il Dr. Federico ETTORI. La loro supervisione durante tutto lo svolgimento del mio lavoro di tesi mi ha appoggiato tantissimo.

Ringrazio anche di cuore il Prof. Paolo BISCARI, che mi ha proposto questo argomento e che mi ha guidato e aiutato durante la totalità del mio periodo al dipartimento, chiarendo qualsiasi mio dubbio che potessi avere. Ringrazio ovviamente anche tutti coloro con cui ho lavorato ogni giorno al dipartimento, con cui ho avuto delle discussioni sempre molto interessanti.

Ringrazio per finire la mia famiglia, i miei amici e compagni di corso che mi hanno supportato tantissimo durante questi due anni di laurea magistrale che ho passato qui al Politecnico. Con questo lavoro finale concludo la mia doppia laurea con l'università francese dell'*École Centrale de Lille*.

Abstract

The scope of this thesis is to simulate the behaviour of anisotropic spin lattices in dynamic conditions, i.e. when a time-varying sinusoidal field is applied. To perform such an analysis, I implemented on MATLAB the Ising model through a dynamic algorithm proposed by NOVOTNY in 1995 that uses a division of the lattice in 18 classes according to the orientation of their nearest-neighbours in horizontal and vertical direction, using the GLAUBER dynamics. After checking that the results yielded by this algorithm in the static case ($B = 0$) are in line with the analytical predictions made by ONSAGER (the anisotropy making the temperature decrease), I computed the dynamic critical temperature with a sinusoidal field of amplitude B_0 and period P, in order to see how T_c evolves with P, B_0 and the anisotropy factor $K = \frac{J_x}{J_y}$, where J_x and J_y are the coupling constants in the horizontal and vertical direction. This allowed to extrapolate some relationships between these parameters and to draw various phase 3D diagrams for the dynamic order parameter, which replaces the usual magnetization in the dynamic case. Finally, in order to account for the disorder present in real physical systems, I introduced the Random Anisotropy Ising Model, in analogy with the Random Bond Ising Model. I then made simulations using this algorithm in order to see the effect of randomness and how it competes with the anisotropy when it comes to the value of the critical temperature.

Keywords : *Ising Model, Glauber Dynamics, Magnetism in Condensed Matter, Phase Transitions, Statistical Physics, Random Bond Ising Model*

Abstract in lingua italiana

Lo scopo di questa tesi è di simulare il comportamento di reticoli di spin anisotropi in condizioni dinamiche, quando un campo magnetico sinusoidale viene applicato. Per eseguire tale analisi, ho implementato su MATLAB il modello di ISING tramite un algoritmo dinamico proposto da NOVOTNY nel 1995 che usa una partizione del reticolo in 18 classi, a seconda dell'orientamento dei loro vicini orizzontali e verticali, usando la dinamica di GLAUBER. Dopo aver verificato che i risultati ottenuti dalle mie simulazioni fossero in linea con le aspettative analitiche previste da ONSAGER nel caso statico ($B = 0$), ho calcolato la temperatura critica dinamica in presenza di un campo variabile con periodo P e ampiezza B_0, per vedere come questa temperatura evolve con P, B_0 e il fattore d'anisotropia $K = \frac{J_x}{J_y}$, dove J_x e J_y sono le costanti di accoppiamento nella direzione orizzontale e verticale rispettivamente. Questo ha permesso di estrapolare alcune relazioni tra questi parametri e di disegnare vari diagrammi di fase tridimensionali per il parametro d'ordine dinamico Q, che si sostituisce alla magnetizzazione M nel caso dinamico. Infine, per tener conto del disordine presente in sistemi fisici reali, ho introdotto il *Random Anisotropy Ising Model*, in analogia con il *Random Bond Ising Model*. Ho effettuato diverse simulazioni usando questo algoritmo per vedere l'impatto della casualità sulla temperatura critica e quanto importante può essere rispetto all'anisotropia.

Parole Chiave : *Modello di Ising, Dinamica alla Glauber, Magnetismo nella Materia Condensata, Transizioni di Fase, Fisica Statistica, Random Bond Ising Model*

Contents

Introduction

The main goal of this thesis is to study how the properties of a two-dimensional $L \times L$ spin lattice abiding by the ISING model are modified when there is some anisotropy in the spin network, i.e. that the interaction between nearest neighbours in the horizontal direction J_x can be different than the one in the vertical direction J_y. Anisotropic 2D spin lattices typically represent physical systems comprised between the ideal one-dimensional case (a finite spin chain) and the ideal two-dimensional case (a perfectly isotropic spin lattice). In particular, we try to analyse how various quantities of interest of such physical systems are being changed when anisotropy comes into play, starting by the static critical temperature.

The dynamics of 2D Ising systems can be simulated using a MONTE-CARLO algorithm. The most simple approach is the single spin-flip algorithm, where all spins are tackled as individual particles. In 1975, LEBOWITZ [17] proposed the 10-fold way algorithm, based on a partition of the spin lattice into classes, a spin pertaining to a given class according to its own orientation and on the orientation of its neighbours. Based on this reasoning, a specific algorithm designed to treat anisotropic two-dimensional lattices that was proposed by NOVOTNY in 1995 [3], using a partition of the lattice in classes, which ultimately improves the computational efficiency with respect to a standard METROPOLIS-HASTINGS algorithm. After a brief theoretical introduction on magnetic materials and on the numerical fondations for the 2D Ising model, we make a review of recent scientific papers that have tackled anisotropic spin lattices with different formalisms and algorithms. After implementing this algorithm, we perform zero-field simulations in order to see how well the data from the simulations reproduces the theoretical behaviour that was predicted by ONSAGER for anisotropic lattices.

Then, we want to study the impact of exerting a time-varying magnetic field on this lattice to see to what extent the properties of the system are modified, thanks to the calculation of the hysteresis loops for different amplitudes and periods of the field, which are two factors that impact the critical temperature.

Thereupon, randomness is introduced in the anisotropy, by analogy with the classical Random Bond Ising Model, in order to see how the random distribution of the bonds competes with a mean anisotropic effect. Eventually, we study the fluctuations of the magnetization for subcritical conditions in order to see to what extent the anisotropy has an impact on the appearance of these fluctuations.

Finally, we study more in depth the link between the anisotropy and the dimensionality of the lattice, to see how well these two concepts can be related between each other, based on the results of our simulations and the scientific literature.

Chapter 1

The Isotropic Ising Model and the Monte Carlo Method

In this first part, after introducing the concepts of magnetism in condensed matter useful to this thesis, namely the magnetic susceptibility and the exchange interaction, we make a description of the ISING model, elaborated by the German physicist Ernst ISING approximately 100 years ago that allows to compute the magnetic response of a ferromagnetic material, namely the phase transition it undergoes. One advantage is that the analytical solutions of the model for the two-dimensional case can be exactly computed within the frame of statistical physics, with the main phenomenon coming into play being the phase transition of the material from a ferromagnetic behaviour to a paramagnetic one. We then show how it can be implemented with the help of a MONTE-CARLO method.

1.1 Phenomenology of magnetic phase transitions in condensed matter

Magnetic materials are primarily characterized by three vectorial quantities :

- the magnetic induction $\overrightarrow{B}$, expressed in Tesla (T);
- the magnetic field $\overrightarrow{H}$, expressed in Amperes per unit length (A/m);

- the magnetization $\overrightarrow{M}$, corresponding to the magnetic moment per unit volume (always null in free space), also expressed in A/m.

In a solid, these quantities are linked mutually by the following linear relationship

$$\overrightarrow{B} = \mu_0(\overrightarrow{H} + \overrightarrow{M}), \tag{1.1}$$

where $\mu_0 \sim 1.257$ H/m is the *vacuum permeability*. The magnetization and the magnetic field are linked in the most general case by the so-called POLDER tensor $\bar{\bar{\chi}}$ which corresponds to the *magnetic susceptibility* :

$$\overrightarrow{M} = \bar{\bar{\chi}}.\overrightarrow{H}. \tag{1.2}$$

However, we can approximate it as a linear relationship between these two quantities, therefore, this POLDER tensor is reduced to a simple scalar coefficient χ if the two vectors are directed along the same axis. If the magnetic susceptibility is positive, the material is considered as paramagnetic. If is negative, the material is called diamagnetic.

These properties depend on the temperature. Indeed, some materials, such as iron (Fe) or cobalt (Co), that exhibit a ferromagnetic behaviour respectively until $T = 1000$ K and $T = 1450$ K. Ferromagnets are materials behaving as permanent magnets, i.e. the magnetization remains non-null even when the applied external field is removed. Once a given temperature T_c, known as the *critical temperature*, is overcome, the ferromagnetic order is destroyed and they become paramagnets, with a zero magnetization. We will interest ourselves for phase transitions from a ferromagnetic behaviour towards a paramagnetic one, i.e. a transition from an ordered state into a disordered one, where the net value of the magnetization acts as the order parameter. This transition is a *second-order* one, with the second derivative of the free energy $\chi = \frac{\partial^2 F}{\partial H^2}$ showing a discontinuity at $T = T_c$, with F the free energy of the system, H the external applied field and χ the magnetic susceptibility, while the first-order derivative $M = \frac{\partial F}{\partial H}$, called the magnetization, shows a continuous behaviour.

Furthermore, ferromagnets are characterized by a so-called 'memory'. Indeed, the curve representing the magnetization as a function of the external field

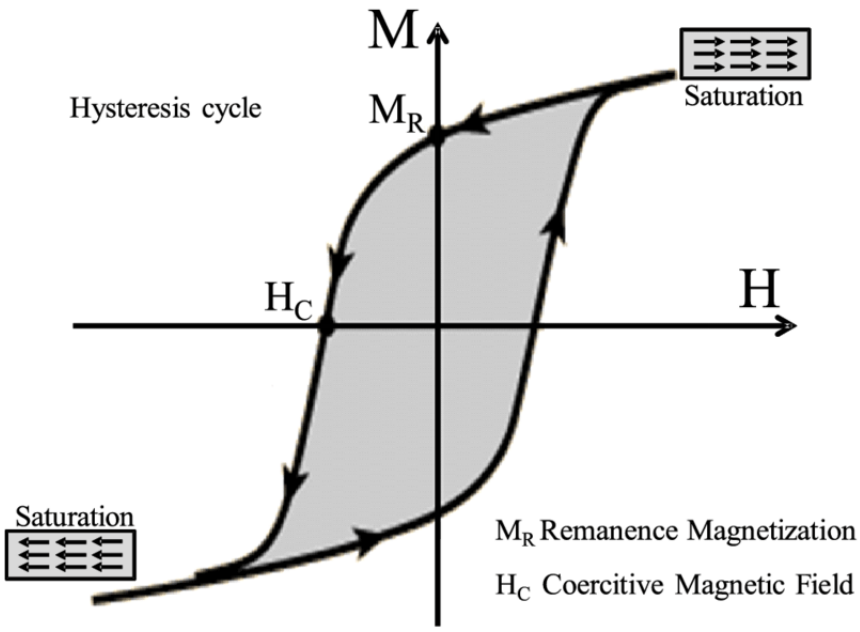

Figure 1.1: Hysteresis loop of a typical ferromagnetic material (R. CARABALLO-VIVAS)

applied shows an *hysteretic* behaviour that can be observed on Fig. 1.1. Let us analyze this curve by starting from the top-right side, where the material is saturated, i.e. its magnetization is the highest possible and can not further increase by increasing the external field H. When bringing the external field to zero, the material will keep a finite value of the magnetization that we call the *remanent magnetization* M_R. To completely demagnetize the sample, we need to apply the so-called *coercive field* H_c, that is necessarily opposed to the magnetization left in the material. The magnetization does not follow the same curve depending on whether the field is increasing or decreasing, hence the term *hysteresis*.

1.2 Exchange interaction

To explain the origin of ferromagnetism, a first intuition would be to think of the *magnetic dipole interaction*, given by the following expression :

$$E_{int} = \frac{\mu_0}{4\pi r^3}\left[\overrightarrow{\mu_1}.\overrightarrow{\mu_2} - \frac{3}{r^2}(\overrightarrow{\mu_1}.\overrightarrow{r})(\overrightarrow{\mu_2}.\overrightarrow{r})\right], \tag{1.3}$$

where $\overrightarrow{\mu_1}$ and $\overrightarrow{\mu_2}$ are the magnetic dipole moments and $\overrightarrow{r}$ is a unit vector parallel to the line linking the two dipoles. However, this energy is generally too weak with respect to the thermal energy and it favours an antiparallel alignment of the spins.

A very relevant phenomenon in magnetic materials is the so-called *exchange interaction*. Let us consider two electrons as independent identical particles and a two-level energy spectrum. This allows us to define two wave functions $\psi_a(r)$ and $\psi_b(r)$ and a joint wave function that reads $\Phi(\overrightarrow{r_1}, \overrightarrow{r_2}) = \psi_a(\overrightarrow{r_1})\psi_b(\overrightarrow{r_2})$. However, this wave function is not suited in this case, since the two particles are considered identical and thus must obey particle exchange according to quantum mechanics. This implies that two new wave functions have to be introduced in order to respect this property :

$$\begin{cases} \psi_S(\overrightarrow{r_1}, \overrightarrow{r_2}) = \frac{1}{\sqrt{2}}\left[\psi_a(\overrightarrow{r_1})\psi_b(\overrightarrow{r_2}) + \psi_a(\overrightarrow{r_2})\psi_b(\overrightarrow{r_1})\right]; \\ \psi_A(\overrightarrow{r_1}, \overrightarrow{r_2}) = \frac{1}{\sqrt{2}}\left[\psi_a(\overrightarrow{r_1})\psi_b(\overrightarrow{r_2}) - \psi_a(\overrightarrow{r_2})\psi_b(\overrightarrow{r_1})\right]. \end{cases} \tag{1.4}$$

These quantities are respectively called symmetric and antisymmetric wave functions and they can be reformulated as follows :

$$\begin{cases} \psi_S(\overrightarrow{r_1}, \overrightarrow{r_2}) = \frac{1}{\sqrt{2}}\left[\psi_a(\overrightarrow{r_1})\psi_b(\overrightarrow{r_2}) + \psi_a(\overrightarrow{r_2})\psi_b(\overrightarrow{r_1})\right]\chi_S; \\ \psi_T(\overrightarrow{r_1}, \overrightarrow{r_2}) = \frac{1}{\sqrt{2}}\left[\psi_a(\overrightarrow{r_1})\psi_b(\overrightarrow{r_2}) - \psi_a(\overrightarrow{r_2})\psi_b(\overrightarrow{r_1})\right]\chi_T, \end{cases} \tag{1.5}$$

where ψ_S and ψ_T are the wave functions of singlet and triplet states, with χ_S and χ_T respectively referring to the orthogonal basis of these states (for the z-component). The singlet and triplet configurations for a two-level energy system are illustrated in Fig. 1.2.

Let us call $\hat{E}$ the Hamiltonian of the two-electron system we consider. We can

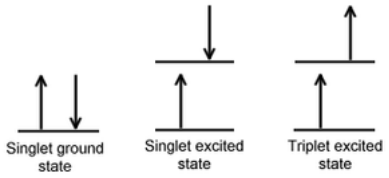

Figure 1.2: Singlet and triplet configurations

define two energy levels associated to the singlet and the triplet states we introduced :

$$\begin{cases} E_S = \int \psi_S^* \hat{E} \psi_S \, d\overrightarrow{r_1} \, d\overrightarrow{r_2}; \\ E_T = \int \psi_T^* \hat{E} \psi_T \, d\overrightarrow{r_1} \, d\overrightarrow{r_2}. \end{cases} \tag{1.6}$$

From these energies, we can define a quantity named the *exchange interaction constant* :

$$J = \frac{E_S - E_T}{2}. \tag{1.7}$$

A ferromagnetic configuration, i.e. that favours the parallel alignment of the spins, will correspond to a lower triplet energy $E_T < E_S$, hence to a positive exchange interaction constant.

1.3 Onsager's analytical derivation

Let us introduce a d-dimensional periodic lattice with $d \in \{1, 2, 3\}$ having for example a cubic or hexahedral shape, forming an array of N sites. Each of these sites corresponds to a given spin configuration $s_i = \pm 1$, $i = 1, ..., N$, the $+$ referring to the *spin-up* state while the $-$ refers to the *spin-down* state. In the following, these two states will be labeled respectively $\uparrow$ and $\downarrow$. The state of the system is given ultimately by the N-tuple $\{s_i\}_{i=1,...,N}$. The ISING Hamiltonian of the system is given by the following expression :

$$H(\{s_i\}_{i=1,...,N}) = -\sum_{i=1}^{N} \sum_{j=1}^{N} J_{ij} s_i s_j - \mu_B B \sum_{i=1}^{N} s_i, \tag{1.8}$$

Figure 1.3: Red-circled grey dots represent the 4 nearest neighbours of the red dot

where B is an external magnetic field, $\mu_B = \frac{e\hbar}{2m_e}$ the BOHR magneton and J_{ij} is the exchange interaction constant for a given pair (i, j). The Ising model considers only nearest-neighbour interactions, as Figure 1.3 shows. Therefore, a lot of terms (all the ones corresponding to non-nearest-neighbour interactions) vanish in the first sum, and the energy becomes $H(\{s_i\}_{i=1,\dots,N}) = -\sum_{\langle i,j\rangle} J_{ij} s_i s_j - \mu_B B \sum_{i=1}^{N} s_i$, in which $\langle i, j\rangle$ designates only the four nearest-neighbour interactions for each spin. For the notice, we consider $\langle i, j\rangle$ and $\langle j, i\rangle$ equivalent. Let us focus on a two-dimensional lattice with constant interaction J for all pairs of nearest neighbours in the absence of an external field ($B = 0$). An analytical solution was found by Lars ONSAGER in 1944. If we consider the magnetization of the system, simply given by :

$$M = \sum_{i=1}^{N} s_i, \tag{1.9}$$

and the mean magnetization per spin

$$m = \frac{\langle M\rangle}{N}, \tag{1.10}$$

where $\langle u\rangle$ is the average of a given physical quantity u within the canonical ensemble in the frame of statistical physics. He showed that the temperature at which the second-order phase transition occurs, also called the CURIE temperature for the 2D ISING model, is given by

$$T_c = \frac{2J}{k_B \ln(1+\sqrt{2})}, \tag{1.11}$$

where k_B is the BOLTZMANN constant. If we make the temperature dimensionless (which is the practical case for computational methods), this yields $\frac{k_B T_c}{J} \simeq 2.2692$. Within the same analytical derivation, ONSAGER also demonstrated that the mean magnetization per spin follows the evolution $m(T < T_c) =$

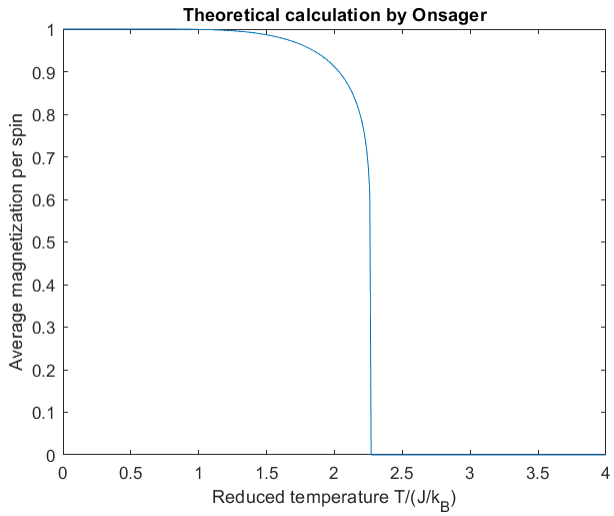

Figure 1.4: Average magnetization per spin according to the ONSAGER's model

$\left[1 - \frac{1}{\sinh^4(\frac{2J}{k_B T})}\right]^{\frac{1}{8}}$ and $m(T > T_c) = 0$, having the evolution pictured by Figure 1.3, which is the expected shape for a second-order phase transition : the magnetization is indeed continuous, but its derivative will exhibit a singularity at the critical point.

For the notice, the ISING model is just a particular case in the study of spin-interacting structures. The most general case can be described by means of the n-vector model, in which the spins are n-dimensional vectors, with n a given integer. For example, in the HEISENBERG model, the spins are three-dimensional vectors, and the Hamiltonian takes the following form :

$$H = -J \sum_{\langle i,j \rangle} \overrightarrow{S_i}.\overrightarrow{S_j}, \tag{1.12}$$

where the scalars in the ISING model are replaced by 3-dimensional vectors $\overrightarrow{S} = (S_x, S_y, S_z) \in \mathbf{R}^3$ and the terms in the sum above correspond therefore to the scalar products between nearest-neighbour spins. The book by STANLEY [5] gives a more detailed overview of such a model. The results presented here will focus on the two-dimensional ISING model, for which $n = 1$ and $d = 2$.

1.4 Statistical mechanics

The ISING model relies on statistical physics, which is a powerful tool to study systems with a large number of interacting particles, in particular to calculate macroscopic quantities of condensed matter systems. Solving the motion equation for each one of the particle would be analytically way too demanding. The approach used here is therefore probabilistic to transition from one state to another, without describing thoroughly all the dynamics. Let us describe this principle. Let μ be the present state of the system we consider. We call $R(\mu \to \nu)$ the probability that it is in a state ν after a given amount of time dt. $R(\mu \to \nu)$ is called the *transition rate*, is expressed in s^{-1} and is assumed to be time-independent. Let us define a set of weights w_μ representing the probability that the system is in a given state μ for a given instant t. The evolution of $w_\mu(t)$ is governed by the so-called *master equation* :

$$\frac{dw_\mu}{dt} = \sum_\nu \Big(w_\nu(t) R(\nu \to \mu) - w_\mu(t) R(\mu \to \nu) \Big), \tag{1.13}$$

considering transitions from and into the state μ. Since the system must be in a given state at every instant t, the sum rule applies and yields $\sum_\mu w_\mu = 1$ for every time t. The *equilibrium state* in this case is obtained by putting the right-hand term of the master equation to 0. The values at equilibrium of the weights will be given by :

$$p_\mu = \lim_{t \to +\infty} w_\mu(t). \tag{1.14}$$

GIBBS demonstrated that for a system in thermal equilibrium with a reservoir at a temperature T, the probability reads $p_\mu = \frac{1}{Z} e^{-\beta E_\mu}$, where E_μ is the energy of the state μ, $\beta = (k_B T)^{-1}$ and $Z = \sum_\mu e^{-\beta E_\mu}$ the partition function, the symbol Z coming from the German word *Zustandssumme*, literally the "sum over the states". From there, we are able to define the *expectation value* of a quantity of interest Q, that will read $\langle Q \rangle = \sum_\mu p_\mu Q_\mu$, hence developing with the above expression for the probability :

$$\langle Q \rangle = \frac{\sum_\mu Q_\mu e^{-\beta E_\mu}}{\sum_\mu e^{-\beta E_\mu}}. \tag{1.15}$$

The limitation of such a calculation tool is that this kind of sum as above can be very hard to derive, especially if the number of states is very large ! This is why there is a need for computational techniques, where we will be able to simulate the evolution of systems of limited size, that we want to increase as much to get as close as possible to the *thermodynamic limit*, above which energy fluctuations could be considered as negligible. In the following section, we will describe the working mechanism of the MONTE-CARLO numerical method, as described in the book by BARKEMA [1].

1.5 The Monte-Carlo method

In the frame of this numerical method, we need to sample the states that we want to study and work with a selected subset, thanks to a probability distribution (p_μ) for example. The formula for the computation of a given physical quantity will therefore be different :

$$Q_M = \frac{\sum_{i=1}^{M} Q_{\mu_i} p_{\mu_i}^{-1} e^{-\beta E_{\mu_i}}}{\sum_{i=1}^{M} p_{\mu_i}^{-1} e^{-\beta E_{\mu_i}}}, \tag{1.16}$$

assuming that there are M selected states $(\mu_1, ..., \mu_M)$. Q_M is the *estimator* of Q. There are a few points to be addressed here : ideally, we should have $M \to +\infty$ since it is the configuration in which the estimator will be the closest to the analytical quantity Q. Furthermore, the probability distribution for the selection of the subset is a crucial choice. We should select states that weigh the most in the sum over the states, according to the BOLTZMANN distribution. The MONTE-CARLO method consists in finding these M most important states, by selecting states for which the probability of being chosen is precisely given by the BOLTZMANN distribution. In this case, the estimator would simply become

$$Q_M = \frac{1}{M} \sum_{i=1}^{M} Q_{\mu_i}. \tag{1.17}$$

For this purpose, it is quite handy to use a so-called MARKOV process to generate a new state ν from a given state μ. The probability of generating that state ν given μ is called the transition probability $P(\mu \to \nu)$. This probability

must always be the same in this frame, regardless of what happened before reaching the state μ, and we should have as well the well-known sum rule $\sum_\nu P(\mu \to \nu) = 1$. It is important to note that we can have $P(\mu \to \mu) \neq 0$. The MONTE-CARLO simulation should therefore consist in a MARKOV process allowing the generation of states appearing with probabilities yielded by the BOLTZMANN distribution, provided it is run for a sufficient time. We will detail below the other conditions that are needed to actually verify this hypothesis.

1.5.1 Ergodicity

The MARKOV process we consider should be able to reach any state of the system, provided it is run for a time long enough. If there is one state ν that can not be reached from a given state μ, that would mean that the probability of reaching it is simply zero, instead of $p_\nu = e^{-\beta E_\nu} \neq 0$.

1.5.2 Detailed balance

The detailed balance condition makes sure that the BOLTZMANN distribution is actually reached for a long enough time of simulation. By putting to 0 the master equation above, we obtain this equation :

$$\sum_\nu p_\mu P(\mu \to \nu) = \sum_\nu p_\nu P(\nu \to \mu). \tag{1.18}$$

By exploiting the sum rule on the left-hand side of this equation, we get $p_\mu = \sum_\nu p_\nu P(\nu \to \mu)$. For any set of transition probabilities satisfying this equation, the probability distribution p_μ will an equilibrium of the dynamics of the MARKOV process. But only satisfying this equation does not imply bindingly that the limit will be p_μ going from any state of the system even if run for long enough. Let us use a matrix formalism to describe the stochastic matrix containing the various transition probabilities $P(\mu \to \nu)$, named $\mathbf{P}$. If we use discrete time steps, the probability of being in the state ν at time $t+1$ is given by $w_\nu(t+1) = \sum_\mu P(\mu \to \nu) w_\mu(t)$, which would become in matrix

notation :

$$\mathbf{w}(t+1) = \mathbf{P}.\mathbf{w}(t), \tag{1.19}$$

this very last equation becoming, provided an equilibrium state is indeed reached :

$$\mathbf{w}(+\infty) = \mathbf{P}.\mathbf{w}(+\infty). \tag{1.20}$$

However, a *dynamic equilibrium* can also be reached, when $\mathbf{w}$ rotates around several values, known as a *limit cycle*. The condition for a very long time will read :

$$\mathbf{w}(+\infty) = \mathbf{P}^{n}.\mathbf{w}(+\infty), \tag{1.21}$$

where n is called the cycle length. If the transition probabilities are chosen so that they respect $p_\mu = \sum_\nu p_\nu P(\nu \to \mu)$, nothing actually guarantees that we will not have any limit cycles, making completely uncertain the fact that the generated states will have the desired probability distribution. To ensure this, we need an extra condition, known as the *detailed balance* :

$$p_\mu P(\mu \to \nu) = p_\nu P(\nu \to \mu). \tag{1.22}$$

This condition allows to get rid of limit cycles. Let us prove this. The left-hand (resp. right-hand) side of this equation corresponds to the overall transition rate from state μ to state ν (resp. ν to μ). Qualitatively, this signifies that on average, the system should go from μ to ν as often as it goes the other way around. For limit cycles however, there must be states for which this condition is not respected on any particular step of the MARKOV chain. Since the probability of occupation of some or all the states varies in a cyclic way, it must happen that some states see their probability of occupation increase, implying that there are more transitions into that state than out of it. Thus, these dynamics are forbidden by the detailed balance condition. Finally, since we want p_μ and p_ν to obey the BOLTZMANN distribution, the detailed balance condition furnishes the following ratio between the two transition probabilities :

$$\frac{P(\mu \to \nu)}{P(\nu \to \mu)} = \frac{p_\nu}{p_\mu} = e^{-\beta(E_\nu - E_\mu)}. \tag{1.23}$$

1.5.3 Acceptance ratio

For the sake of simplicity, the transition probability is written in the following way :

$$P(\mu \to \nu) = g(\mu \to \nu)A(\mu \to \nu), \tag{1.24}$$

where $g(\mu \to \nu)$ is the selection probability and $A(\mu \to \nu)$ is the acceptance ratio telling whether the system will go into the newly generated state ν. Therefore, the general principle of a MONTE-CARLO algorithm is to generate random new states ν from old ones μ with a probability $g(\mu \to \nu)$ and then accept or not the move with an acceptance ratio $A(\mu \to \nu)$, having to fulfill the detailed balance condition :

$$\frac{g(\mu \to \nu)A(\mu \to \nu)}{g(\nu \to \mu)A(\nu \to \mu)} = e^{-\beta(E_\nu - E_\mu)}. \tag{1.25}$$

In the particular case of the n-fold algorithm we use, we will see that this probability is always equal to 1.

Chapter 2

The Anisotropic Ising Model and the Lebowitz - Novotny algorithm

2.1 Anisotropic spin lattices in past scientific literature

An anisotropic spin lattice is a spin network in which the interaction between a spin and its two nearest neighbours in the horizontal direction J_x can be different from the one between this spin and its nearest neighbours in the vertical direction J_y, as illustrated on Fig. 2.1. From a theoretical point of view, in the absence of an external magnetic field, ONSAGER [7] demonstrated that for a given lattice of size $N_x \times N_y$ with horizontal (resp. vertical) exchange interaction J_x (resp. J_y), the critical temperature fulfills the following condition

$$\sinh\Big(\frac{2J_x}{k_B T_c}\Big)\sinh\Big(\frac{2J_y}{k_B T_c}\Big) = r, \tag{2.1}$$

with $r = \frac{N_x}{N_y}$ a quantity called the aspect ratio. In the case of a square lattice, we have $r = 1$. This equation can be solved numerically and yields the expected theoretical value of T_c for a given arrangement (J_x, J_y).

Anisotropic spin lattices and their implementation, in the last 20 years, have been tackled in several scientific papers that investigated various ways to determine critical parameters of such systems. M. GHAEMI, M. GHANNADI and B. MIRZA [13] computed in 2003 the critical temperature of a multi-layer ferromagnet with anisotropic exchange interaction, using the numerical

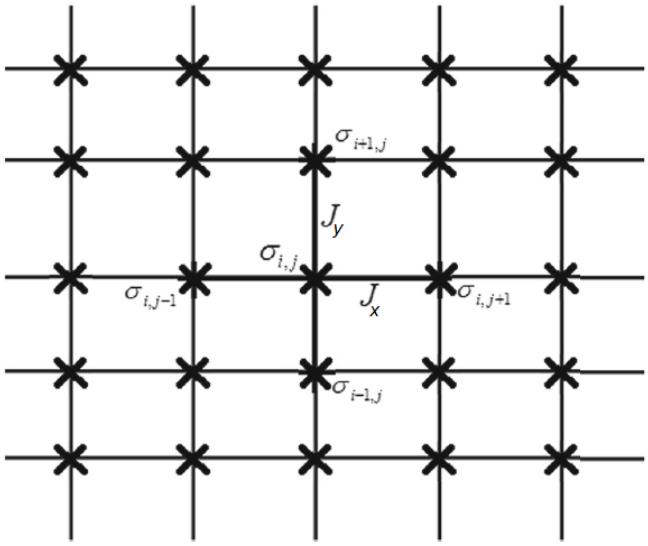

Figure 2.1: A schematic representation of an anisotropic spin lattice [14]

Transfer Matrix Method. They defined three coupling variables : the in-plane exchange constants K_x and K_y (that correspond to J_x and J_y we introduced in the previous chapter) and the inter-layer coupling constant K_z and used the Transfer Matrix method. To determine the critical temperature, they plotted the reduced internal energy per site as a function of the reduced temperature for different lattice sizes. These curves crossing themselves at the critical point, this allows to recover this parameter. They calculated this parameter for various values of the in-plane anisotropy ratio $\rho = \frac{K_y}{K_x}$ and $\xi = \frac{K_z}{K_x}$. The graph in Fig. 2.2 shows the computed values within this model for T_c as a function of ρ for different values of the parameter ξ. As we can observe, for a fixed value of ξ, the critical temperature diminishes as the in-plane anisotropy factor ρ increases, in a similar fashion for all three values of ξ. Clearly, the in-plane anisotropy, which will be our focus in this thesis (we will simulate 2D lattices) has a higher impact than the inter-layer one : the three curves are pretty close from one another, despite the variation of ξ.

In 2017, D. FARSAL, M. SNINA, M. BADIA and M. BENNAI studied anisotropic spin lattices by the means of two methods : the Finite-Cluster Approximation (FCA) and the Monte-Carlo algorithm. By computing the magnetic susceptibility and finding the position of its peak, they confirmed that the critical temperature undergoes a decreasing trend when the anisotropy goes up, as

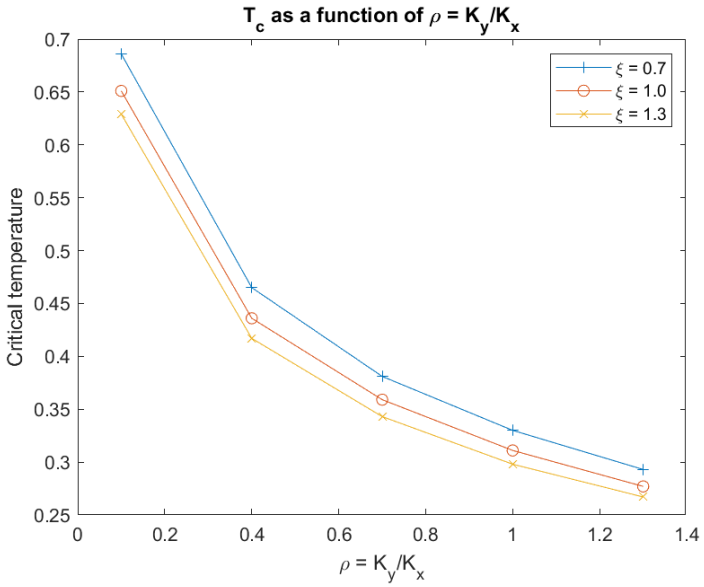

Figure 2.2: Calculation of the critical temperature by GHAEMI [13] as a function of the anisotropy

Fig. 2.3 shows.

They also obtained the phase diagram (between the ordered phase $T < T_c$ and the disordered phase $T > T_c$) presented in Fig. 2.4, which shows $\frac{J_v}{T_c}$ as a function of $\frac{J_h}{T_c}$ in the theoretical case (i.e. as predicted by ONSAGER), the mean-field approximation, the FCA approach and the Monte-Carlo simulation. J_h and J_v represent the variables we introduced as J_x and J_y in our work. As we can see, the results of the Monte-Carlo simulation are pretty well in line with the theoretical expectation by Onsager. The mean-field and the FCA are pretty far from the analytical expectation, although the FCA reproduces the trend pretty well. The Monte-Carlo method used in this paper is the classical single-spin flip static algorithm, i.e. one spin is flipped at a time.

In 2019, MURTAZAEV and IBAEV [15] studied the Anisotropic Ising Model with competing interactions with nearest neighbours (ANNNI) using the WANGLANDAU algorithm. This article again confirms the essential fact regarding the anisotropic lattices : the critical temperature decreases when the coupling constants Jx and Jy get very different from one another.

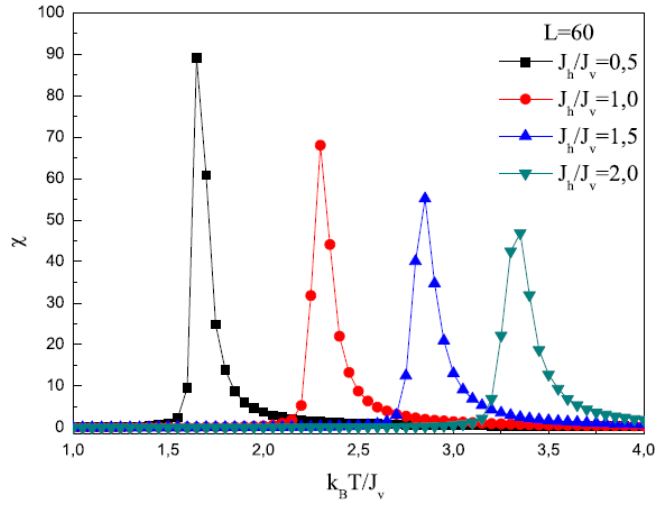

Figure 2.3: Magnetic susceptibility for different anisotropies (lattice size L = 60) [14]

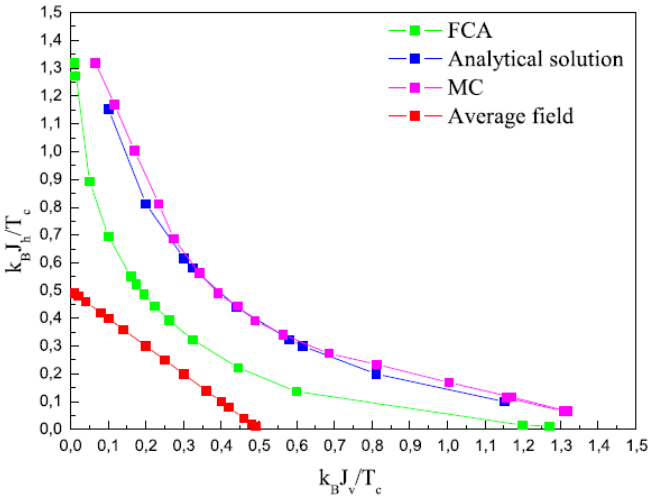

Figure 2.4: Phase diagram with four different methods [14]

2.2 The n-fold way algorithm

2.2.1 The n-fold partition of the lattice

Let us consider an *anisotropic* spin lattice of size $L_x \times L_y$, in which the exchange interaction in the horizontal direction J_x and the one in the vertical direction J_y are not necessarily equal. The ISING Hamiltonian for an anisotropic lattice reads :

$$H(\{s_i\}) = -J_x \sum_{i=1}^{L_x} \sum_{j=1}^{L_y} s_{i,j} s_{i+1,j} - J_y \sum_{i=1}^{L_x} \sum_{j=1}^{L_y} s_{i,j} s_{i,j+1} - \mu_B B \sum_{i=1}^{L_x} \sum_{j=1}^{L_y} s_{i,j}. \quad (2.2)$$

The usual MONTE-CARLO algorithm is the following :

1. Start from an initial spin configuration;
2. Choose a random spin to flip among the $L_x \times L_y$ that are in the grid;
3. Compute the probability that it will flip (this will be addressed this);
4. Choose a uniformly distributed number r comprised between 0 and 1. If $r \leqslant p$, do $s_{i,j} \leftarrow -s_{i,j}$;
5. Increment the time by one time step;
6. Return to step 2 and iterate.

In 1975, LEBOWITZ [2] proposed a new way of implementing the MC algorithm, in order to make it more computationally efficient. It is based on the fact that we can make a partition of our spin lattice into several classes, according to how many $\uparrow$ nearest neighbours a spin has. For an isotropic lattice, we count $n = 10$ classes to characterize all possible nearest-neighbour configurations. In the anisotropic case, as it has been described by NOVOTNY [3] in 1995, the spins will be classified as in the table 2.1 (with exactly $n = 18$ classes describing exhaustively the lattice), alongside with the energy change of the system if the flipping actually occurs. For the notice, the magnetic field B is applied in the negative direction, and its sign has been taken into account for the computation of the different energy shifts $\Delta E = E_{old} - E_{new}$.

Class	Initial spin	Horizontal ↑ n.n.	Vertical ↑ n.n.	Energy shift ΔE
1	+1	2	2	$-4J_x - 4J_y + 2\lvert\mu_B B\rvert$
2	+1	2	1	$-4J_x + 2\lvert\mu_B B\rvert$
3	+1	2	0	$-4J_x + 4J_y + 2\lvert\mu_B B\rvert$
4	+1	1	2	$-4J_y + 2\lvert\mu_B B\rvert$
5	+1	1	1	$2\lvert\mu_B B\rvert$
6	+1	1	0	$4J_y + 2\lvert\mu_B B\rvert$
7	+1	0	2	$4J_x - 4J_y + 2\lvert\mu_B B\rvert$
8	+1	0	1	$4J_x + 2\lvert\mu_B B\rvert$
9	+1	0	0	$4J_x + 4J_y + 2\lvert\mu_B B\rvert$
10	-1	2	2	$-4J_x - 4J_y - 2\lvert\mu_B B\rvert$
11	-1	2	1	$-4J_x - 2\lvert\mu_B B\rvert$
12	-1	2	0	$-4J_x + 4J_y - 2\lvert\mu_B B\rvert$
13	-1	1	2	$-4J_y - 2\lvert\mu_B B\rvert$
14	-1	1	1	$-2\lvert\mu_B B\rvert$
15	-1	1	0	$4J_y - 2\lvert\mu_B B\rvert$
16	-1	0	2	$4J_x - 4J_y - 2\lvert\mu_B B\rvert$
17	-1	0	1	$4J_x - 2\lvert\mu_B B\rvert$
18	-1	0	0	$4J_x + 4J_y - 2\lvert\mu_B B\rvert$

Table 2.1: 18-fold classification of the spins for an anisotropic configuration.

This algorithm uses the same dynamics as the standard one, i.e. a single spin-flip. The main difference between the standard algorithm and the n-fold way algorithm is that while in the standard one, we choose a spin and decide to flip it according to a given probability p. in the n-fold way, however, the spin flipping is performed certainly at each step of the algorithm. The selection of the spin that will flip depends on the class configuration of the current spin lattice. In contrast to the usual method, the increment of time elapsed between each MC iteration is variable and will depend on a random number and on the number of spins that have each p value, that is the population of each class reported in the table 2.1. The main advantage of this algorithm is that unlikely events are reached in a lesser amount of CPU time, which allows to have a better computational speed at low T.

2.2.2 Absorbing Markov chains

Let us introduce the concept of absorbing MARKOV chains, which are relevant for the implementation of the n-fold way algorithm. In an absorbing MARKOV chain, there is at least one *absorbing state*, meaning that if the system gets in this state, it will remain there forever. Let us use a basic example to illustrate this feature, with Alice and Bob playing a game with a 10-side dice, on which two sides are labeled "Alice wins", one side "Bob wins" and all the 7 others "Roll the dice again". Let us write the transition matrix associated to this game, having state 1 :"Alice wins", state 2 : "Bob wins" and state 3 "Roll the dice again" :

$$M = \begin{pmatrix} 1 & 0 & 0 \\ 0 & 1 & 0 \\ 0.2 & 0.1 & 0.7 \end{pmatrix}, \tag{2.3}$$

which constitutes indeed a MARKOV matrix, since the matrix is not dependent of the previous states of the system. The two first rows of this matrix represent what we call an absorbing state : once they are reached, the game is over and the dice is not rolled again. For the notice, all rows have their sum equal to unity, since one state of the dice is bindingly up at all times. Let us focus on the initial state : the system must necessarily be in the state corresponding to the unit vector $v^{\mathbf{T}} = [0, 0, 1]$. We can prove that after m rounds of the game, the probability of being in one of the three states of the system is the 3-tuple $p_m = v^{\mathbf{T}}.M^m$. Let us consider the probability that Alice has won the game after m steps, that will be given by the following sum : $p_{A,m} = 0.2 + 0.2 \times 0.7 + ... + 0.2 \times 0.7^{m-1}$. By using the formula for the geometric sum, we obtain $p_{A,m} = \frac{2}{3}(1 - 0.7^m)$, this implying that the probability that Alice wins after a very large number of steps ($m \to +\infty$) is $\frac{2}{3}$. Let us now transpose this to the n-fold way problem. We label n_i the number of spins in a given class $i = 1, ..., n$. If we name N the total number of spins, we have of course $\sum_{j=1}^{n} n_j = N$. Therefore, the quantity $\frac{n_j p(j)}{N}$ is the probability of choosing a spin in class j and flipping it, $p(j)$ corresponding to the probability that if a spin in class j is chosen, it will flip. Let us then build the $(n+1) \times (n+1)$-sized matrix that will correspond

to the MARKOV process associated to this process. Similarly to the 3×3 example presented above, we will have a lower-right diagonal element that will give the probability of remaining in the current spin configuration, while all the other diagonal elements will give the probability of being absorbed, this corresponding in this case to exiting the current spin configuration. The transition matrix will have the following shape :

$$M_{n+1,n+1} = \left[\begin{array}{c|c} \mathbf{I}_{n\times n} & \mathbf{0}_{n\times 1} \\ \hline \mathbf{R}_{1\times n} & \lambda \end{array}\right], \tag{2.4}$$

where $\mathbf{I}_{n\times n}$ is the identity matrix, $\mathbf{0}_{n\times 1}$ is a zero n-tuple, λ is a scalar and $\mathbf{R} = \frac{1}{N}[n_1 p(1), ..., n_n p(n)]$. Since it is a MARKOV matrix, we should have the following relation for the last row :

$$\lambda = 1 - \frac{1}{N}\sum_{j=1}^{n} n_j p(j), \tag{2.5}$$

λ corresponding to the probability of remaining in the current spin configuration. We choose the following notation $\lambda = 1 - \frac{Q_n}{N}$. The probability of remaining in the current spin configuration after m time steps is λ^m, similarly to the "roll the dice again" situation in the previous example. Instead, the probability of an absorption (i.e. exiting the current configuration) is given by $\lambda^{m-1}(1-\lambda)$. Let us choose a random number $\tilde{r}$ such that $0 < \tilde{r} \leqslant 1$. This number corresponds to the value of the probability when the system exits the current spin configuration, and the equation $\lambda^{m-1} \geqslant \tilde{r} > \lambda^m$ yields the number of time steps m required to flip this probability. Since λ is by definition smaller than 1, the resolution of this inequality gives the following relation :

$$m - 1 \leqslant \frac{\ln \tilde{r}}{\ln \lambda} < m, \tag{2.6}$$

thus preventing the number $\tilde{r}$ to be zero. The probability of absorption into a particular class will be given by $A = \frac{1}{Q_n}[n_1 p(1), ..., n_n p(n)]$. Let us form the partial sums $Q_i = \sum_{j=1}^{i} n_j p(j)$ for i=1,...,n, putting $Q_0 = 0$. To decide which class will be interested by the flipping, we need to find the integer $k \in \{1, ..., n\}$ such that :

$$Q_{k-1} \leqslant r Q_n < Q_k, \tag{2.7}$$

where r is a random number generated from a random distribution in the interval $[0, 1[$. In case there are several spins in the chosen class, an extra randomization has to be carried out in order to perform the single spin-flip. Assuming that $\frac{Q_n}{N} \ll 1$, we can recover the time increment needed for exiting the current spin configuration, that will be given by :

$$\Delta t = -\frac{N}{Q_n} \ln \tilde{r}. \tag{2.8}$$

2.2.3 Implementation and choice of the dynamics

The algorithm for the 18-fold way method will have the following steps :

1. Choose an initial spin configuration and set the accumulated time to zero;
2. Generate a random number $\tilde{r}$ and increment the accumulated time by the suitable time increment given by Equation (2.8);
3. Choose a random number r and determine which class k satisfies the above inequality. If there are several spins in the class, generate a new random number to choose which spin to flip. Perform $s_{i,j} \leftarrow -s_{i,j}$;
4. Change the class of the chosen spin by adding ± 9 modulo 18 to its previous class number if the flipped spin was initially $\uparrow$ (resp. $\downarrow$);
5. Change the class of the two nearest neighbours in the horizontal direction by adding 3 modulo 18 if the flipped spin was initially $\uparrow$ (-3 if $\downarrow$);
6. Change the class of the two nearest neighbours in the vertical direction by adding 1 modulo 18 if the flipped spin was initially $\uparrow$ (-1 if $\downarrow$);
7. Return to step 2 and iterate.

Some arrays are useful to keep track of all the quantities that we have mentioned when we proceed to the practical implementation. The first one is the array $\mathcal{C}$, of size 18×1, such that $\forall i = 1, ..., 18, \mathcal{C}(i) = n_i$. Taking $N = L_x \times L_y$, we have then the two-dimensional array **LOC** of size $N \times 18$ that contains the location of the spins in the lattice for each class we consider. The two

other arrays are **LOOK**, giving the index of the first dimension in **LOC**, and **LOOC** giving the class number of a spin given its position $i \in \{1, ..., N\}$ in the lattice having been made one-dimensional. This leads to the relationship $\mathbf{LOC}(\mathbf{LOOK}(i), \mathbf{LOOC}(i)) = i$. It is noteworthy that only the $\mathcal{C}(k)$ spins in the column $\mathbf{LOC}(j, k)_{j=1,...,\mathcal{C}(k)}$ contain the spin locations in current use.

Let us then explain the dynamics that were used in order to choose the probability of selection and flipping of a given spin. In this case, the usual METROPOLIS-HASTINGS dynamics, where

$$p = \min\left\{1, e^{\frac{\Delta E}{k_B T}}\right\}, \tag{2.9}$$

were not employed, instead, we used the so-called GLAUBER dynamics, where the probability p reads :

$$p = \frac{1}{1 + e^{-\frac{\Delta E}{k_B T}}}, \tag{2.10}$$

where $\Delta E = E_{old} - E_{new}$. The advantage of this method over the METROPOLIS-HASTINGS dynamics is that the actual value of the energy shift ΔE is always considered, whereas the METROPOLIS dynamics allows with equal probability (1 in this instance) all flips such that the energy of the system decreases. Instead, the GLAUBER dynamics favours, for a fixed temperature T, the flips that induce a higher ΔE, as shown on the figure 2.5.

In the computational implementation, we will use transition rates, i.e. probabilities per unit time, expressed in s^{-1}. In the frame of the GLAUBER dynamics, we can show that it is written :

$$w_i(s_j) = \frac{1}{2\alpha}\Big(1 + s_j \tanh(\beta \frac{\Delta E_i}{2})\Big), \tag{2.11}$$

where α is the inverse of a time determining the time scale of the process and $s_j = \pm 1$ is the numerical value of the spin we consider. In our 18-fold model, we will therefore dispose of 18 transition rates, corresponding to each one of the spin classes we consider. With this, we are set to launch the simulation, provided that we can compute our measurable quantities, such as the magnetization, the latent heat or the magnetic susceptibility.

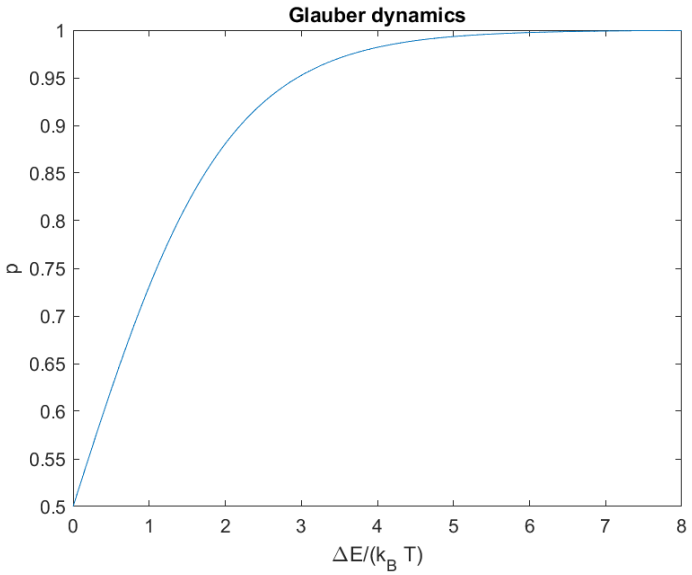

Figure 2.5: $p = f(\Delta E)$ for the GLAUBER dynamics

2.3 Impact of the anisotropy on T_c

2.3.1 Physical phenomenon and analytical expectations

Increasing the anisotropy of the system, i.e. making the ratio $K = \frac{J_x}{J_y}$ bigger, will tend to gradually transform the two-dimensional lattice into a one-dimensional one. Let us consider a $(N+1)$-spin 1D ferromagnetic chain. The exchange Hamiltonian reads as usual $H = -2J\sum_{i=1}^{N} s_i s_{i+1}$. Adding one defect in the chain, i.e. a spin that is not aligned to the other ones, will cost an energy $E = J$, whereas the entropy will read $S = k_B \ln N$, since the defect can be placed on N different positions along the chain. Therefore, considering the free energy $F = E - TS$, the defect formation will cause F to diverge towards $-\infty$ when the chain becomes infinitely long for any $T > T_c$, preventing any ordered configuration for the one-dimensional case. There is no phase transition in the 1D case, or rather we can say that it occurs for $T = 0$. This implies that we should observe a decrease in $T_c(K)$ as the anisotropy ratio K is increasing.

To determine the critical temperature for a given configuration of the lattice, that is a given size $N = L \times L$ (we consider square lattices) and a given anisotropy $K = \frac{J_x}{J_y}$, we first need to adapt our reference system for the tempera-

ture proceeding to a normalization of our exchange interaction J : let us write $J_x = \sqrt{2}J\cos\alpha$ and $J_y = \sqrt{2}J\sin\alpha$. Indeed, this allows to be independent of which way we define the anisotropy, i.e. whether J_y (resp. J_x) increases with respect to J_x (resp. J_y) This means for example that $\frac{J_x}{J_y} = 2$ should be equivalent to $\frac{J_y}{J_x} = 2$. We have a new form for our exchange interaction $J = \frac{J_x^2+J_y^2}{2}$, for which the directionality will be determined by the angle α. The rotation from $\alpha = \frac{\pi}{4}$ to $\alpha = 0$ marks the transition from a fully isotropic lattice towards a completely one-dimensional one. Furthermore, we can demonstrate analytically that for $\alpha \to 0$ (or $\pi/2$, which is equivalent), we have $T_c \to 0$. Indeed, for $\alpha \to 0$, thanks to usual considerations on the equivalents ($\cos(\alpha \to 0) \sim 1$, $\sin(\alpha \to 0) \sim \alpha$ and $\sinh(X \to 0) \sim X$), we have

$$\frac{2\sqrt{2}J}{T_c}\sinh\Big(\frac{2\sqrt{2}J}{T_c}\Big) = \frac{1}{\alpha}, \tag{2.12}$$

yielding $\lim_{\alpha\to 0} T_c(\alpha) = 0$. The input variable of our algorithm is the anisotropy factor K, implying within this formalism that the values of J_x and J_y are derived thanks to the angle $\alpha = \text{arccotan}(K)$. The temperature will now be expressed as units of $\frac{1}{k_B}\sqrt{\frac{J_x^2+J_y^2}{2}}$. For the sake of simplicity, we take numerical values for J and k_B equal to 1. This formalism allows to recover the well-known value as found by ONSAGER $T \simeq 2.26$ for $J_x = J_y$. Let us look at the equation (2.12) from a graphical point of view, in order to confirm that the critical temperature is indeed decreasing when the anisotropy is increasing and that for any $0 \leqslant p \leqslant 1$, $\alpha_1 = p\frac{\pi}{2}$ and $\alpha_2 = (1-p)\frac{\pi}{2}$ we have exactly the same T_c, since α_1 and α_2 correspond to anisotropy factors K and $1/K$, both representing the same physical configuration. We see on Figure 2.6 that the critical condition is reached as expected for $T \simeq 2.26$ in the isotropic case ($\alpha = \pi/4$) whereas the curves for equivalent anisotropy $(0, \pi/2)$ and $(\pi/8, 3\pi/8)$ are overlapped and their crossings with the horizontal line $f = 1$ are shifted towards lower temperature with respect to the isotropic lattice.

2.3.2 Computation of the physical quantities

We first need to compute the magnetic susceptibility χ. Physically it represents how easily the material will respond to a magnetic excitation by an external

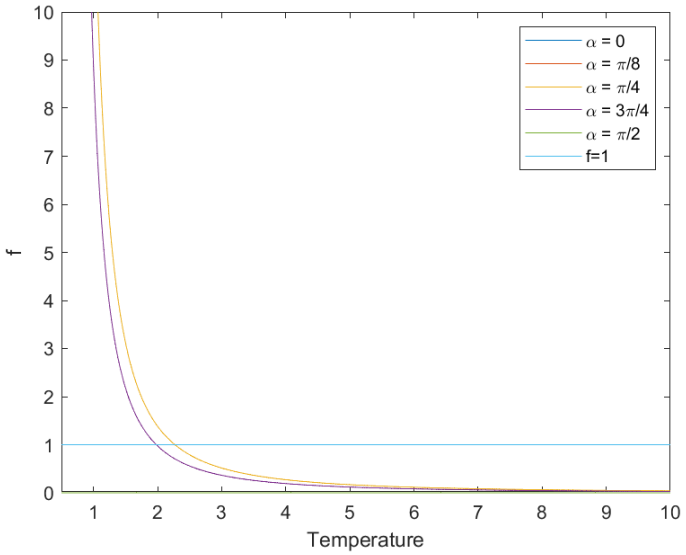

Figure 2.6: Graphical determination of the expected critical temperature, with $f(T) = \sinh\left(\frac{2J_x}{k_B T}\right)\sinh\left(\frac{2J_y}{k_B T}\right)$

field. It is in the most general case a tensor, but in the most simple case, $\overrightarrow{M} = \chi.\overrightarrow{H}$. We know that for a paramagnetic material, i.e. for $T > T_c$, this quantity will be proportional to the inverse of the temperature, more exactly it will have the following evolution :

$$\chi = \frac{C}{T - T_c}, \tag{2.13}$$

where C is a temperature-independent multiplicative constant. This implies that for a 2D ferromagnet, the magnetic susceptibility exhibits a singularity at the critical temperature.

To compute this quantity numerically, we use the following relationship :

$$\chi(T) = \beta(\langle m^2 \rangle - \langle |m| \rangle^2), \tag{2.14}$$

where $\langle m^2 \rangle$ corresponds to the average squared magnetization per spin, m^2 being computed at each MC step alongside m, and $\beta = \frac{1}{k_B T}$. Another quantity of interest is the fourth-order BINDER cumulant, calculated in the following way :

$$U_4(T, N) = 1 - \frac{\langle m^4 \rangle}{3\langle m^2 \rangle^2}, \tag{2.15}$$

related to the *kurtosis*, that is the "tailedness" of the order parameter m. It is a very useful quantity since for a given anisotropy coefficient, the different curves of $U_4(N)$ as a function of the temperature should all cross in a unique point, of which the x-coordinate is the critical temperature T_c, allowing to perform a double-check with the value we found using the peak of the magnetic susceptibility.

To define the stopping criterium for this 18-fold MONTE-CARLO algorithm, we need to define a maximum elapsed time above which we stop the program, indeed, using a *for* loop is not suited since we can not predict how many time steps we will have, the time increments depending on random numbers generated at each new iteration. Therefore, a *while* loop is used to run this iterative algorithm, stopping when the imposed maximum time has been reached.

2.3.3 Results of the simulation

We first need to fix a total time **TimeMax** during which the system will evolve and that will be the ending condition for the *while* loop mentioned above, i.e. when the total elapsed time has overcome the value of this parameter. We took in all the simulations **TimeMax** $= 10000$, which turned out to be a good compromise between the computational speed and the simulation time required to reach equilibrium for the measurable quantities of interest we are looking at, such as the magnetization or the global energy of the system.

The graphs on Figure 2.7a and 2.7b show the typical evolution of these quantities for a ferromagnetic state ($T < T_c$) with an anisotropy $K = 2$ (corresponding to an angle $\alpha = \text{cotan}(2) \sim 0.4636\text{rad}$). The equilibrium configuration is reached since we see that the energy is stationary around a negative value, indicating it is a favourable configuration for the system, while the magnetization per spin reaches a steady state as well, very close to 1 in absolute value, indicating that the spin lattice is very strongly directed in one direction, as we can see on Figure 2.8 (with the $\uparrow$ spins in white and the $\downarrow$ ones in black). This plot implies that the critical temperature for $K = 2$, as we will check later, is higher than $T = 1.9$, since we obtain an ordered configuration with a large majority of the spins that are aligned, whereas the paramagnetic behaviour

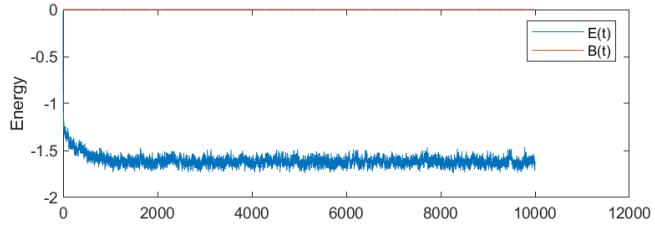

(a) Energy

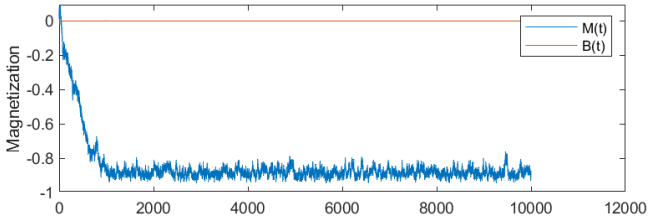

(b) Magnetization

Figure 2.7: Simulation realized for K = 2 and T = $1.9\frac{J}{k_B}$ (L = 100)

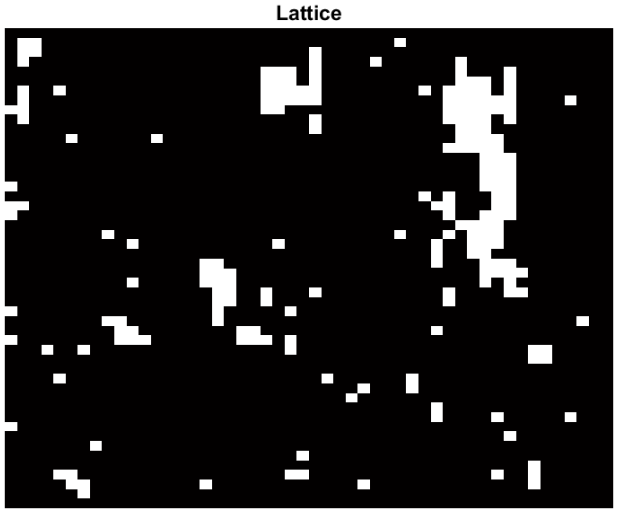

Figure 2.8: Lattice at the end of the simulation for K = 2 and T = $1.9\frac{J}{k_B}$ (L = 50)

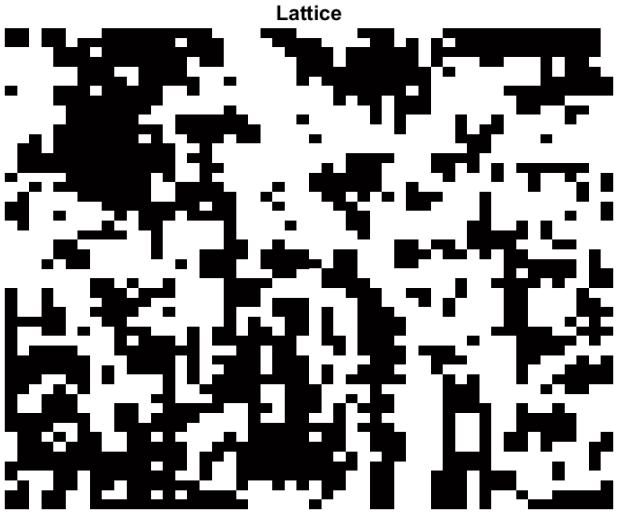

Figure 2.9: Lattice at the end of the simulation for $K = 2$ and $T = 2.7\frac{J}{k_B}$ ($L = 50$)

above T_c would favour an eventual lattice configuration as the one shown on Figure 2.9 : here we talk about a *disordered* state, in which no particular orientation of the spins is preferred. The mean magnetization per site will be close to zero in such situations and we can deduce from this equilibrium configuration that the critical temperature for the $K = 2$ case is lower than $2.7\frac{J}{k_B}$.

Then, the key quantity for the knowledge of the state of system is the *average magnetization per spin*, labeled as $\langle m \rangle$. To obtain it, we need to make a temporal average of the magnetization per spin once the system has entered equilibrium. To increase the reliability of the value obtained, we can run the experiment multiple times and average the temporal mean values obtained themselves to weaken as much as possible the random component of the simulation, while $\langle m^2 \rangle$ and $\langle m^4 \rangle$ are also computed in the same way.

After having computed the order parameter of the system and some of its moments, we want to see the evolution of the thermodynamic quantities such as the magnetic susceptibility χ alongside the temperature. The temperature loop was executed in a decreasing way, using the equilibrium lattice at the temperature $T + \Delta_T$ as the initialization lattice at the temperature T This allows to avoid as much as possible metastable configurations, since an anisotropic lattice can present so called *striped configurations* below the critical temperature and thus have a mean magnetization per spin lower

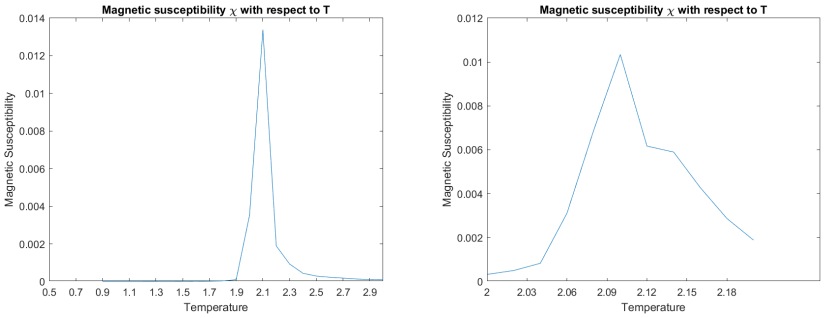

(a) $\Delta T = 0.1 \frac{J}{k_B}$ **(b)** $\Delta T' = 0.02 \frac{J}{k_B}$

Figure 2.10: Peak of the magnetic susceptibility for $L = 100$

than 1, which would make the computation of the magnetic susceptibility meaningless, since we must have a clear transition from 1 to 0.

To obtain reliable results, we first made a temperature sweep in the calculation of the magnetic susceptibility with a step $\Delta T = 0.1 \frac{J}{k_B}$ in a large interval, in order to have a first estimate of the position of the peak, and then we refine it around a narrower interval (typically of length $0.2 \frac{J}{k_B}$) centered around our first estimation with a more accurate temperature step $\Delta T' = 0.02 \frac{J}{k_B}$, as it is illustrated on the figures 2.10a and 2.10b, for the case of a 100×100 lattice with a $K = 2$ anisotropy. In this case, we have a first estimate of the position of the peak around $T = 2.1$ that we refined to finally confirm it was $T = 2.10$, with a sensitivity of $\Delta T' = 0.02$. We repeated the process for various values of the anisotropy factor, refining it particularly around $\alpha = \frac{\pi}{4}$. We then compared it to the analytical curve given by the equation (2.1), thanks to which we recover T_c with the MATLAB solver for a given angle α. Figure 2.11 shows the superposition of both plots. As a first observation, the fitting between both graphs seems good. However, we notice that the analytical curve shows finite values for the temperature even at very low angles (that is at high anisotropy factor K). For $K = 80$, we obtain $T_c \sim 0.754$, which is still far from zero. Indeed, taking a very small angle such as $\alpha = 10^{-12}$ yields again a finite temperature $T_c \sim 0.113$. The graph in Figure 2.12 shows on a semi-logarithmic scale the evolution of T_c for extremely small values of the angle α, down to 10^{-36}, where we still get a finite temperature $T_c = 0.0357$. Below this threshold, the solver runs into an error. To have a reference for a comparison, we can try to get an estimate of the critical temperature for very

small values of the angle α. Making suitable approximations, we get

$$T_c \sim \frac{2\sqrt{2}}{2\sqrt{2} - \ln(\alpha) - \ln(\ln(\frac{1}{\alpha}))}, \tag{2.16}$$

which we can write under an even more approximate form for small α using the dimensional quantities :

$$\frac{k_B T_c}{J} = -\frac{2\sqrt{2}}{\ln(\alpha)} + O_{\alpha\to 0}\Big(\frac{\ln(\ln(\alpha))}{\ln(\alpha)}\Big). \tag{2.17}$$

We see on Figure 2.12 that this analytical estimation gives a fair estimate of the solutions computed by the solver for the critical temperature, up to an angle $\alpha \sim 10^{-25}$, where the gap between the curves gets significantly higher. For each value of the anisotropy factor, the position of the magnetic

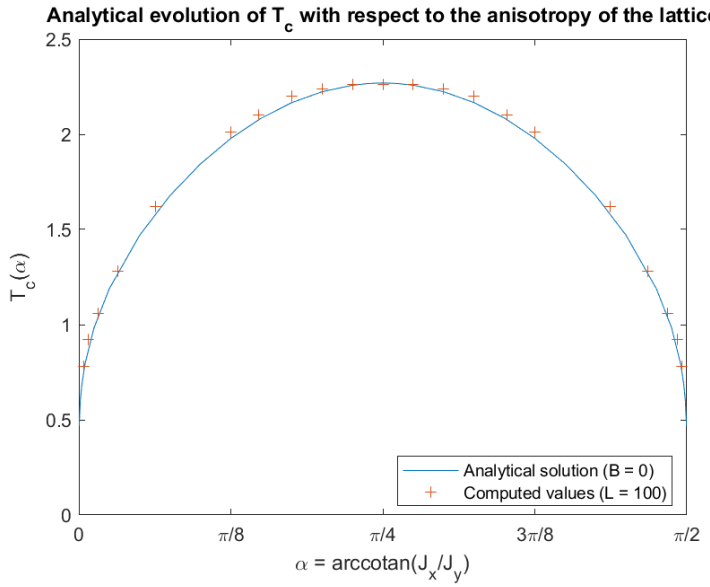

Figure 2.11: $T_c = f(\alpha)$ (analytical and computed values)

susceptibility's peak was cross-checked with the position of the crossing point of the BINDER cumulants for several lattice sizes, as Fig. 2.13 shows in the case $K = 2$.

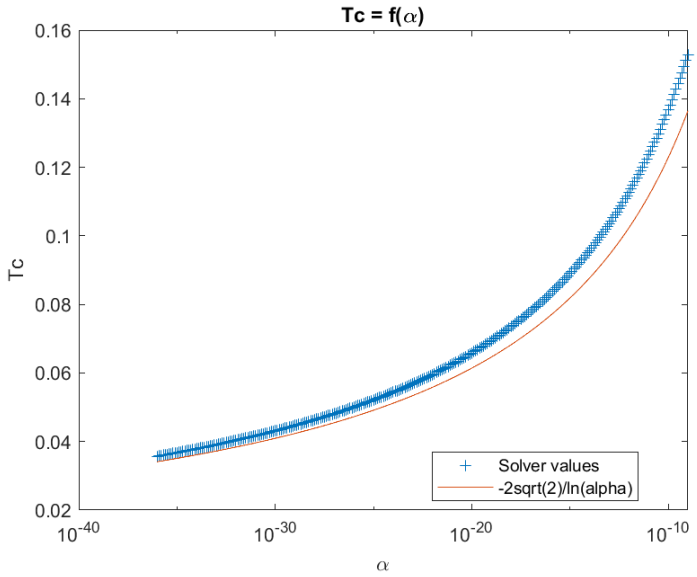

Figure 2.12: $T_c = f(\alpha)$ for very large anisotropies (solver values and analytical approximation)

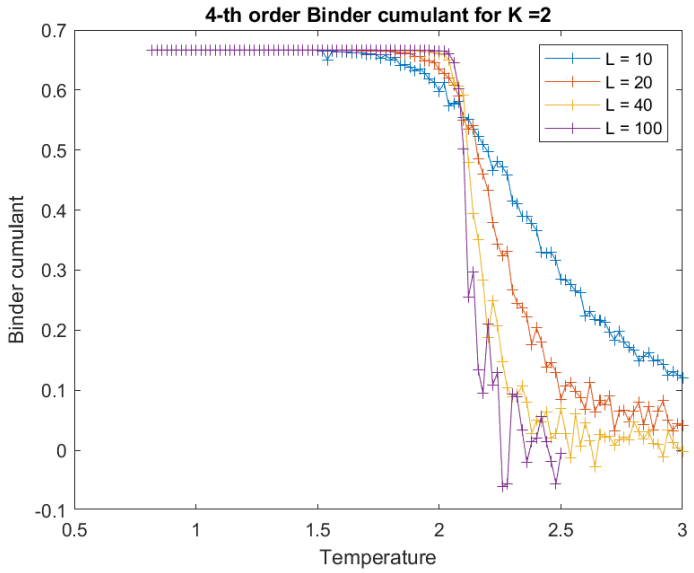

Figure 2.13: Verification of the critical temperature for $K = 2$ with the crossing point of the BINDER cumulants

Chapter 3

Dynamic Phase Transitions in anisotropic Ising Systems

Until now, we have worked only in absence of an external magnetic field $B = 0$, in order to simulate the spontaneous properties of anisotropic ferromagnetic materials. However, an interesting feature that we can add to the anisotropic framework is the presence of an oscillating field with a given time period P. In this chapter, we will highlight how the properties of our system are impacted by the presence of a variable field and how they "compete" with the anisotropy of the system, as the articles by CHAKRABARTI [8] and YÜKSEL [9] did.

3.1 The dynamic order parameter Q

The Hamiltonian of the system remains the same as in the time-independent case, with the only difference that $B = B(t)$ is now a function of time :

$$H(\{s_i\}) = -J_x \sum_{i=1}^{L_x} \sum_{j=1}^{L_y} s_{i,j} s_{i+1,j} - J_y \sum_{i=1}^{L_x} \sum_{j=1}^{L_y} s_{i,j} s_{i,j+1} - \mu_B B(t) \sum_{i=1}^{L_x} \sum_{j=1}^{L_y} s_{i,j}, \quad (3.1)$$

where $B(t) = B_0 \cos(\frac{2\pi}{P} t)$. The objective is the same as in the static case, i.e. identifying the critical conditions. To do this, we need to define a quantity

named the *dynamic order parameter* :

$$Q = \frac{1}{P} \oint M(t) dt, \tag{3.2}$$

where $M(t)$ is the instantaneous magnetization of the system and $\oint$ denotes the integral performed over a full period of the magnetic field. Q is also called the *average magnetization per cycle*. We obviously have Q comprised between 0 and 1, since the absolute value of the magnetization is itself comprised between 0 and 1 at each time step. Let us take the two extreme cases that could occur with a time-varying magnetic field from a phenomenological point of view :

- if the material is perfectly paramagnetic, the magnetization will be proportional to the magnetic field at each time step t. Therefore, $M(t)$ will be a sinusoidal curve in phase with $B(t)$ and its integral over a period will be 0. This is the *dynamic disordered phase*;
- instead, if the material is insensitive to the magnetic stimulation and its magnetization remains unchanged at a value 1, then the order parameter will be equal to 1. We call it the *dynamic ordered phase*.

The presence of a dynamic component of our system implies the existence of two configurations :

- for fixed period and intensity of the magnetic field, we can study the evolution of the dynamic order parameter as a function of the temperature, so as to determine the critical temperature T_c when the system is subject to an oscillating field. We expect the critical temperature to decrease in this case for a fixed anisotropy, since the oscillating field can be seen as a perturbation bringing disorder to the system and thus lowering T_c;
- for a fixed temperature ($T < T_c$) and fixed field's intensity, we can evaluate the critical period of the magnetic field, i.e. the one below which the magnetization can not follow anymore the magnetic field, that we note analogously P_c.

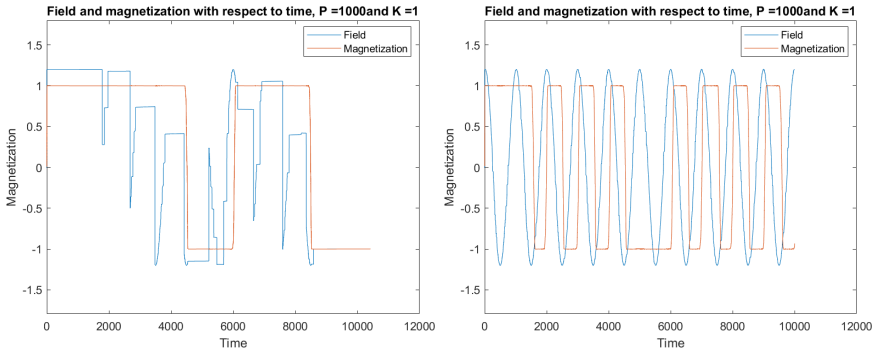

(a) Without modifying the algorithm **(b)** Modifying the algorithm

Figure 3.1: Temporal evolution of $B(t)$ and $M(t)$ over 10 periods for $K = 1$ and $T = 0.7$

The algorithm needs to be modified as well. Indeed, what happens at very low temperature (typically below $0.6\frac{J}{k_B}$) is that the time increments Δt we calculate at each step are very high and can be even higher than the period of the magnetic field we give as input to the algorithm. Therefore, the subsequent magnetization of the system would make not much sense. To resolve this, we apply an extra step in the MONTE CARLO algorithm, which consists in the following alternative :

- if $\Delta t \leqslant \frac{P}{50}$, the spin flipping is accepted as in the standard algorithm and the total elapsed time is incremented by Δt;
- else, the spin flipping is not performed *but* the time is still incremented, in this case by $\frac{P}{50}$.

The threshold $\frac{P}{50}$ has been chosen by performing empirical tests. Fig. 3.1a and Fig. 3.1b show an example of the magnetization and the magnetic field with the standard algorithm and with the modified one for the temperature $T = 0.7\frac{J}{k_B}$.

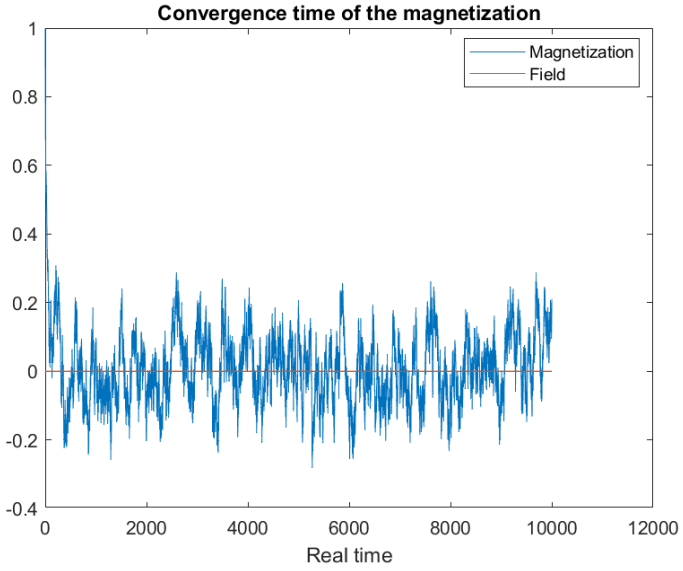

Figure 3.2: Convergence of the system in the absence of a magnetic field

3.2 Fixed period P

3.2.1 Evolution of the critical temperature

Substantially, the algorithm remains completely unchanged with respect to the static case. The only difference is that the time-varying field needs to be updated properly at each time step, since we are using a varying time increment Δt. It is also important to note that our 18-fold algorithm remains completely applicable here, since at each time step, the magnetic field assumes a fixed value, therefore the 18 classes yielding the energy variation for each time step of the simulation are always well defined.

We first need to choose a proper temporal period for the magnetic field we apply. To determine it, let us simulate the evolution of a fully magnetized lattice at a temperature $T > T_c$ for a given anisotropy and see how long it needs to converge to the zero-magnetization state. This experiment is shown on Fig. 3.2. We notice that the time needed to get into the non-magnetized state ($\bar{M} = 0$) after starting in the fully magnetized state ($\bar{M} = 1$) is approximately 500. We choose a period $P = 1000$ to make sure that transitions from a dynamically disordered phase from a dynamically ordered one (diminishing the temperature) actually happen.

Let us look at different cases for the evolution of the magnetic field and the magnetization along time, with $P = 1000$ and $B_0 = 0.3$, with a lattice size $L = 50$, depicted in the four graphs in Fig. 3.3.

Let us analyze each of the four plots. In Fig. 3.3a, for $T = 1.1$, the material is dynamically ferromagnetic : despite the time-varying oscillating field, the lattice remains almost completely magnetized in an only direction. Increasing the temperature to $T = 1.8$ like in Fig. 3.3b, we see that the behaviour of $M(t)$ has changed a lot : the magnetization oscillates between -1 and 1 with the same period than the magnetic field, however with a slight phase delay. When we increase again the temperature ($T = 2.8$), the in-phase oscillations of the field and of the magnetization are almost perfect in Fig. 3.3c, the amplitude of the magnetization having decreased. The most extreme case is depicted by the last figure Fig. 3.3d, where the amplitude of the magnetization is now lower than the one of the magnetic field (indeed, it gets to 0 as the temperature increases) but the phase difference is now 0. Interestingly, we notice the increasing importance of noise as the temperature increases in the magnetization curves, due to the increasing contribution of thermal noise. However, this should not have a big impact on the computation, since we perform calculations of averaged quantities. Therefore, after averaging a curve like the one shown on Fig. 3.3d over a large number of periods, this eliminates the bias of the thermal agitation.

If we perform the computation of the dynamic order parameter over a suitable temperature range, we obtain the plot shown in Fig. 3.4 for $K = 2$, where the dynamic critical temperature here is clearly identifiable as $T_{c,d} = 1.50$ (the resolution in temperature is here $\Delta T = 0.05$), which is *smaller* than the ideal critical temperature we computed without an external magnetic field, which was $T_c \sim 2.076$. This confirms the fact that the time-varying magnetic field acts as a disorder agent on the lattice, thus lowering the actual critical temperature. To precisely determine the critical temperature, we can use the variance of Q, which will be given by

$$\mathcal{V}(Q) = L^2(\langle Q^2 \rangle - \langle |Q| \rangle^2), \tag{3.3}$$

and, similarly with the magnetic susceptibility in the static case, will yield a

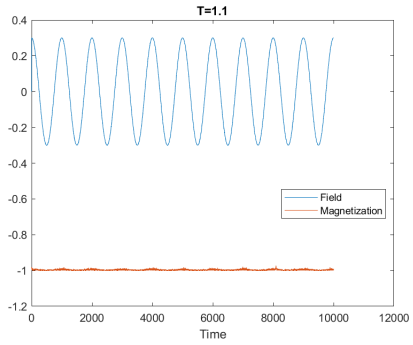

(a) $T = 1.1\frac{J}{k_B}$

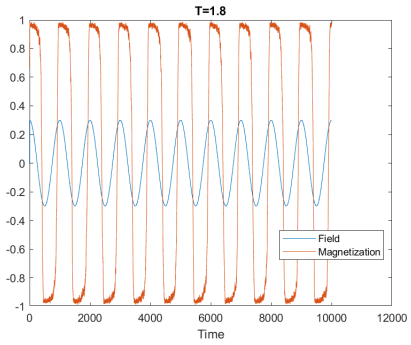

(b) $T = 1.8\frac{J}{k_B}$

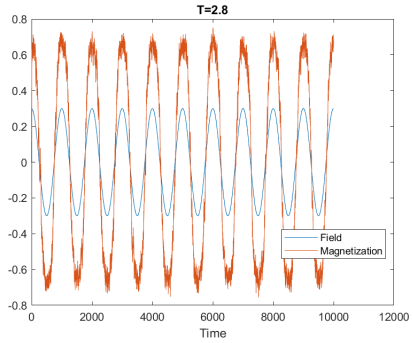

(c) $T = 2.8\frac{J}{k_B}$

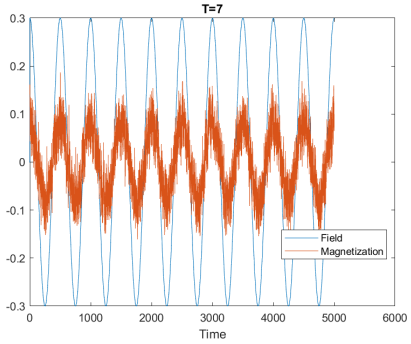

(d) $T = 7\frac{J}{k_B}$

Figure 3.3: Illustration of different steps of a dynamic phase transition ($K = 2$ and $P = 1000$) : magnetization and field are shown as a function of time

peak at the position of the dynamic critical temperature, as can be observed in Fig. 3.5, in the case of a 30×30 lattice with anisotropy $K = 1$ and a magnetic field $(B_0 = 0.3, P = 1000)$.

Applying the same computation for different anisotropies, we can enrich the graph $T_c = f(\alpha)$ shown on Fig. 2.11 with the values of the dynamic critical temperatures. The graph on Fig. 3.6 shows to what extent the curve of the critical temperature as a function of the anisotropy angle $\alpha = \text{arccotan}(\frac{J_x}{J_y})$ is shifted towards lower values when a time-varying magnetic field is present. The effect is clearly visible at the center of the graph, for low anisotropies, where the gap between the critical temperature in the zero-field case and the critical temperature under a time-varying magnetic field can be as high as $0.5\frac{J}{k_B}$. When the anisotropy is increasing, we observe that the gap between the critical temperature and the dynamic critical temperature is getting weaker but the dynamic critical temperature is still smaller than the one in the zero-

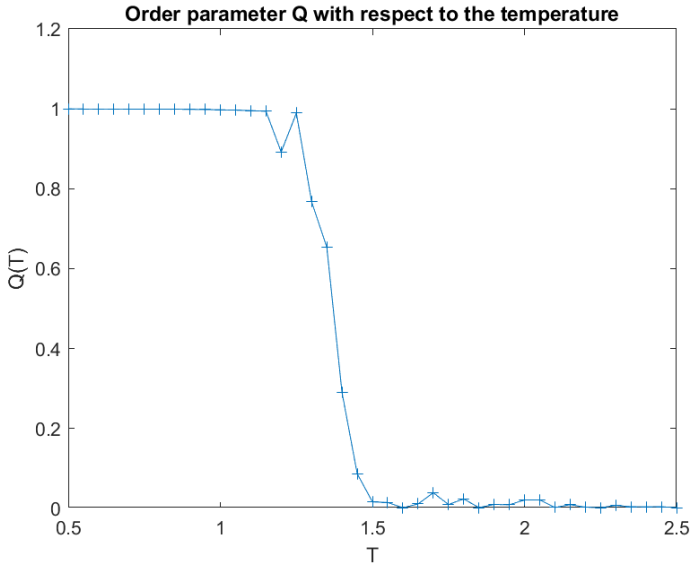

Figure 3.4: Dynamic order parameter Q as a function of T (K = 2)

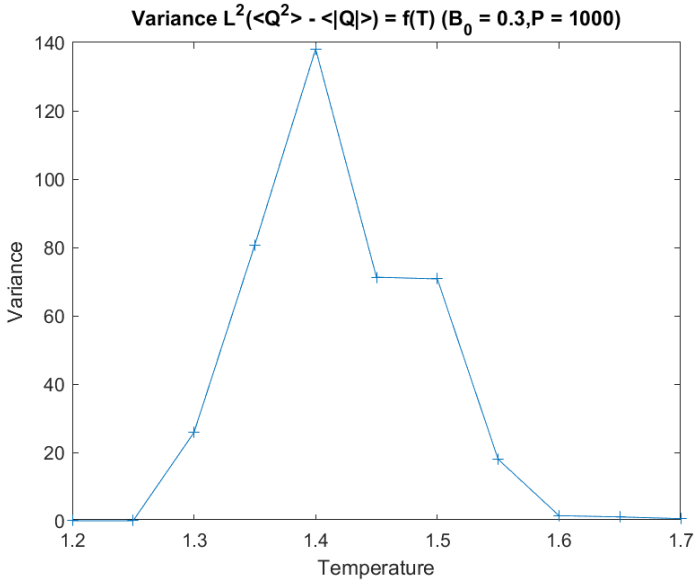

Figure 3.5: Variance of the dynamic order parameter $\mathcal{V}(\mathrm{Q})$ as a function of temperature

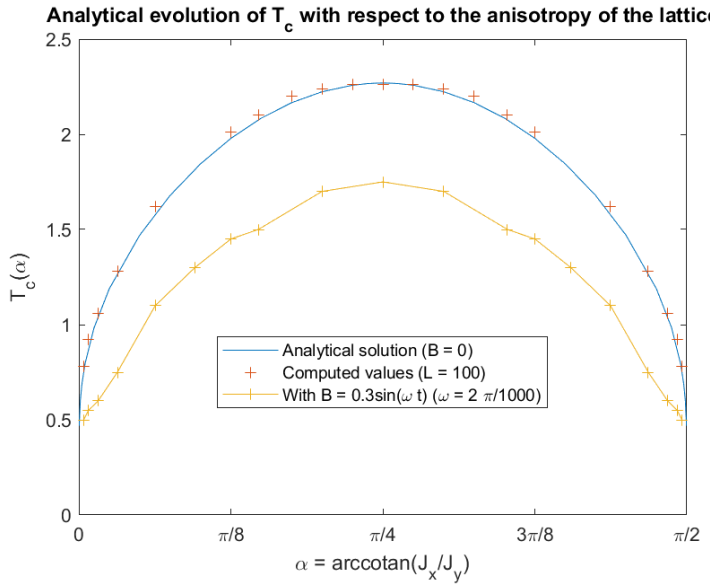

Figure 3.6: Critical temperature as a function of the anisotropy with and without the presence of time-varying magnetic field)

field case.

3.2.2 Evolution of the $M - H$ curve

An other figure of merit of the time-varying ISING system is the evolution of the magnetization as a function of the applied field, the so-called $M - H$ curve. Indeed, for a given temperature, we can obtain this plot from the time curves of the external field and of the magnetization by collecting at each time step over a period P the tuple $(H(t), M(t))$. Let us look at various $M - H$ curves for an anisotropy $K = 2$ for example. The several plots are shown in Fig. 3.7.

These four plots show very well the various phases through which our system goes when the temperature changes. First, for very low temperatures, such as $T_1 = 0.9\frac{J}{k_B}$, we have a mean magnetization per site equal to unity all along time, causing the $M - H$ curve to look like Fig. 3.7a. Then , when the temperature increases, an *hysteretic* behaviour appears : this is the sign that both the magnetization and the field oscillate, but with a phase difference as in Fig. 3.7b : the system has already entered the dynamic paramagnetic state. As the temperature increases again, we see that the phase difference

decreases in such a way that the hysteretic loop has a decreasing area (Fig. 3.7c). Finally, when the temperature is high enough (Fig. 3.7d), the hysteresis loop disappears and the $M - H$ curve turns into a straight line : the magnetization is completely in phase with the magnetic field.

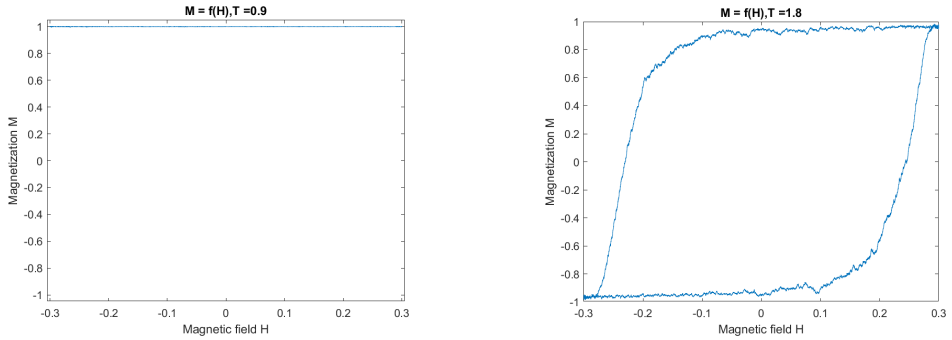

(a) $T = 0.9\frac{J}{k_B}$ **(b)** $T = 1.8\frac{J}{k_B}$

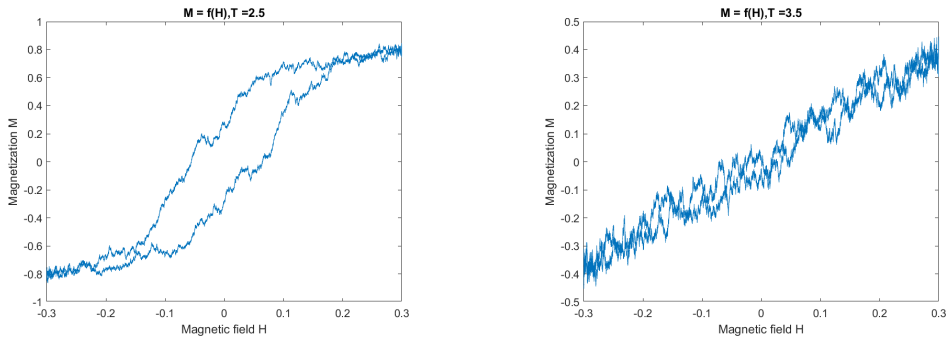

(c) $T = 2.5\frac{J}{k_B}$ **(d)** $T = 3.5\frac{J}{k_B}$

Figure 3.7: Evolution of the $M - H$ curve along temperature ($K = 2$)

To study quantitatively this evolution, we need to define a numerical parameter : for example, the loop area $A = \oint M(H)dH$ (we can obtain this value with the MATLAB command **polyarea**(H,M), with H and M being the values of the magnetic field and of the magnetization sampled over a period). Before plotting this quantity for different values of the anisotropy, let us try to predict its evolution : according to the curves displayed in Fig. 3.7, it seems that A should have almost zero values for low and high T, where no loop behaviour is present, while it should reach its highest point for intermediate values of the temperature.

Let us look at the curves $A(T)$ for different values of the anisotropy factor

K presented in Fig. 3.8. As expected, the temperature corresponding to the maximum loop area is shifted towards lower values when the anisotropy is increasing, in concordance with Fig. 3.6. Furthermore, we can compare the x-coordinate of the loop area peak with the dynamic critical temperatures we found looking at the curves of the dynamic order parameters and we indeed check that they coincide.

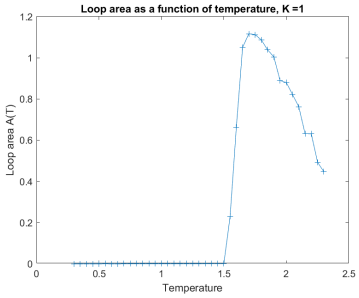

(a) K = 1

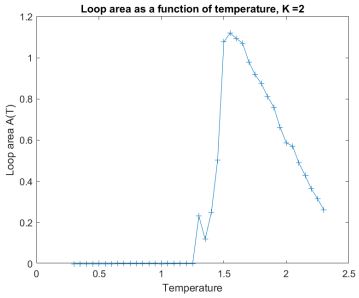

(b) K = 2

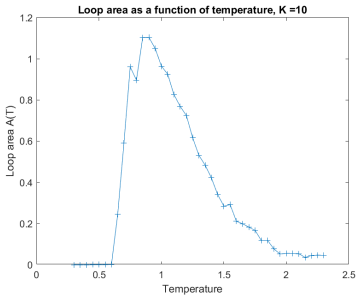

(c) K = 10

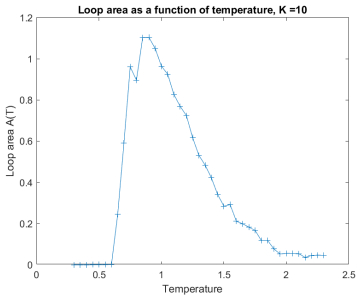

(d) K = 40

Figure 3.8: Loop area A as a function of the temperature for several anisotropy factors K

3.3 Fixed temperature T

The other case we are interested in is to recover a quantity named the *critical period* of the dynamic system. Indeed, for a given temperature, the variation in the frequency of the time-varying magnetic field will cause the dynamic order parameter $Q = \frac{1}{P}|\oint M(t)dt|$ to vary as well. Let us think quantitatively about what should happen. For high frequencies, i.e. short periods of the magnetic fields, the magnetization struggles to follow the magnetic field and can't reverse itself as fast as the field does. Therefore, the dynamic order parameter will be maximum in such a configuration. Instead, if the period of the field increases, the system will tend to a slower dynamic and the magnetization will become more and more able to follow the dynamics of the oscillating field. Thus, we expect the dynamic order parameter to go to zero as the frequency diminishes.

3.3.1 Evolution of the critical period with anisotropy

To evaluate how the critical period goes with the anisotropy and below which value of P the magnetization is not able anymore to follow the magnetic field, we made a frequency sweep for the excitation signal (the time-varying magnetic field) for the usual values of K (1, 2, 5, 10, 20, 40 and 80) so as to observe the dynamic order parameter as a function of the period. We place ourselves for each anisotropy at a temperature $T^* = 0.8T_c(K)$, which turns out to be a good compromise for the computation : below T^*, the magnetization goes to 1 for all periods of the field so it is impossible to draw a phase transition, whereas for temperatures too close or higher than $T_c(K)$, the magnetic field always follows the magnetic field, so that the order parameter is always 0 and makes it as well impossible to plot a phase transition. Fig. 3.9 shows an example of a phase transition for the $Q - P$ curve in the case $K = 2$. We used a step $\Delta P = 20$ for the period. For a given period, the total time of the simulation is chosen equal to **TimeMax** $= 5P$ and the average magnetization per cycle is calculated over 4 periods. Furthermore, the order parameter stored and plotted in Fig. 3.8 is averaged over five independent runs, so as to eliminate unwanted bias.

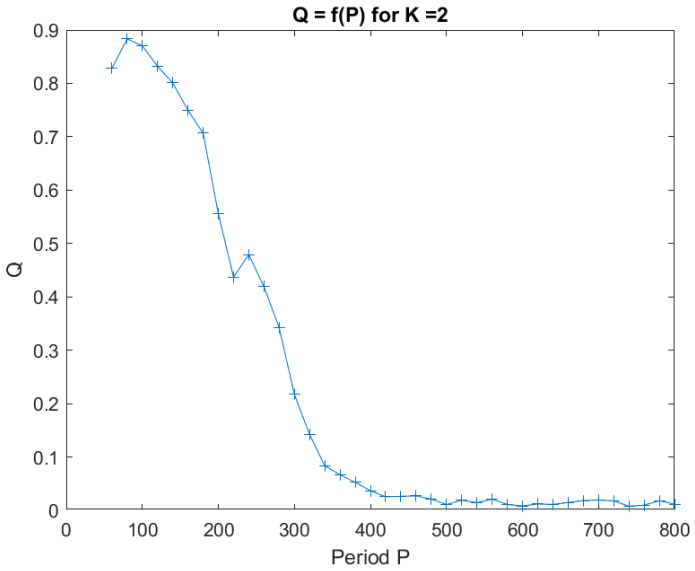

Figure 3.9: Dynamic order parameter as function of the period ($T^* = 0.8T_c(2) = 1.661$)

We obtain the curves $Q = f(P)$ for various anisotropies in order to see how the critical period $P_c(K)$ changes when K increases. Four different phase transitions, each of them at a temperature $T^*(K) = 0.8T_c(K)$, are shown in Fig. 3.10. We observe that the critical period of the system, i.e. the temperature over which the dynamic order parameter is zero, decreases when the anisotropy increases. Let us then investigate, as for the temperature-wise study, the evolution of the loop area as a function of the period (or the pulsation) for various anisotropies.

3.3.2 Evolution of the $M - H$ curve

Again fixing the temperature value at $T^*(K) = 0.8T_c(K)$, we now want to investigate what happens to the evolution of the magnetization as a function of the magnetic field over a full cycle of the field. Let us observe the looks of the hysteresis curves for various values of the period of the external magnetic field. Fig. 3.11 shows six different cases for the $M - H$ curve in the case of a weak anisotropy ($K = 2$). When the period is very small ($P = 20$) as shown in Fig. 3.11a, the magnetization does not follow the magnetic field and remains at a high value, close to 1, therefore the hysteresis is almost non-existent and

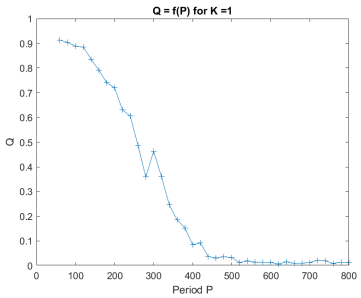

(a) $K = 1$

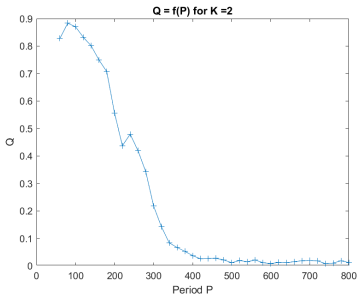

(b) $K = 2$

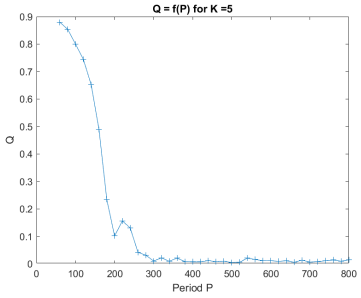

(c) $K = 5$

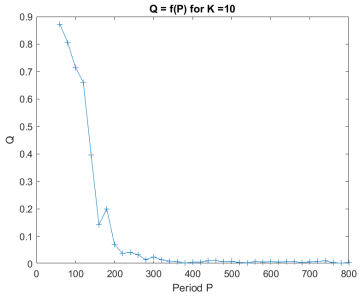

(d) $K = 10$

Figure 3.10: $Q = f(P)$ for various values of the anisotropies ($T^*(K) = 0.8T_c(K)$)

the loop area is consequently very close to 0. Increasing the period ($P = 50$) as in Fig. 3.11b, the loop area increases and the center of the hysteresis is closer to 0, as we can see on Fig. 3.11c. Around $P = 500$, the hysteresis curve reaches a maximum and is well centered around the origin of the graph. This means that the dynamic order parameter has reached an almost null value, as it can be observed on Fig. 3.9. Increasing again the period for $P = 900$ and $P = 5000$, respectively Fig. 3.11e and 3.11f, we see that the loop area is progressively decreasing, though remaining well above zero even for high periods.

Let us then look at the evolution of the loop area $A = f(P)$ (calculated in the same way as in the previous section with **polyarea**(H,M)) for different anisotropies, in order to see if a common pattern emerges.

As we can observe on Fig. 3.12, the plots $A = f(P)$ show a very sharp increase for low periods ($P < 500$) until they reach a maximum almost equal to the full occupancy of the grid (which corresponds to 1.2 in this case, since the values of the field are comprised between -0.3 and 0.3). This maximum is reached

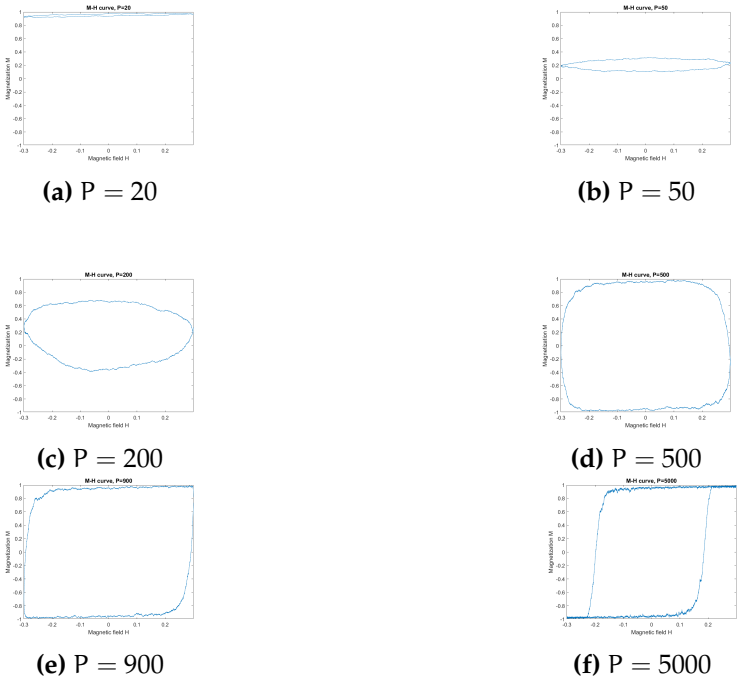

(a) $P = 20$ **(b)** $P = 50$

(c) $P = 200$ **(d)** $P = 500$

(e) $P = 900$ **(f)** $P = 5000$

Figure 3.11: Evolution of the $M - H$ hysteretic behaviour for different values of P ($K = 2$)

for the same value of the period for all anisotropies we considered, that we can identify to $P^* \sim 500$. Furthermore, the curves are almost superimposed in this first domain. We can interpolate it with a linear trend shown by the black line on Fig. 3.13 (based on the mean points between the four different anisotropy factors in the increasing domain of the loop area).

Then, once the extremum is passed, as we see on Fig. 3.12, they evolve in a distinct way, though all decreasing in a progressive way, with a $\frac{1}{x}$-like fashion (to which a constant term is added). This means that the phase shift (i.e. time delay) between the magnetic field and the magnetization is decaying very slowly. Interestingly, we notice that when the anisotropy increases, the loop area decreases more rapidly with respect to the field period (for a given period P, the loop area is always the smallest for $K = 20$ in the decreasing part of the plot).

In order to reverse our perspective, we can also visualize the loop area as a function of the angular frequency $\omega = \frac{2\pi}{P}$ as plotted on Fig. 3.14. For high frequencies, we notice that the loop area for weak anisotropies ($K = 1, 2$) gets closer to 0 with respect to higher values of K, again with a single peak

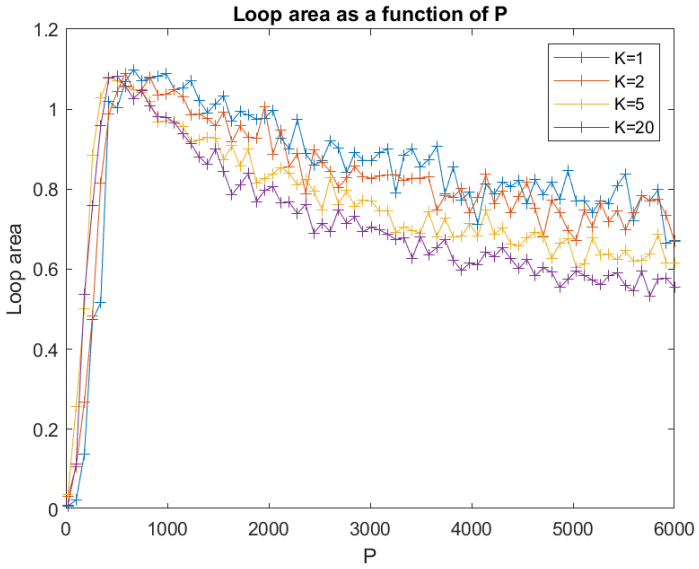

Figure 3.12: Loop area A as a function of the magnetic field's period P

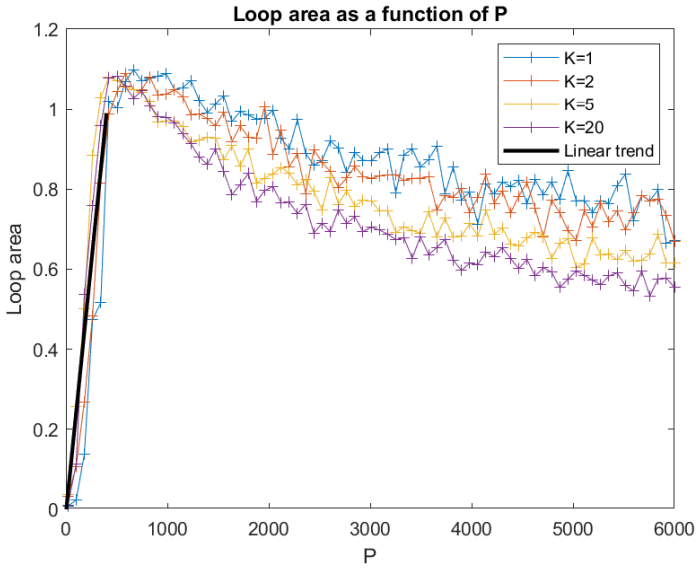

Figure 3.13: Loop area A as a function of the magnetic field's period P with the average linear trend ($a = 0.0025$ and $b = -0.01$)

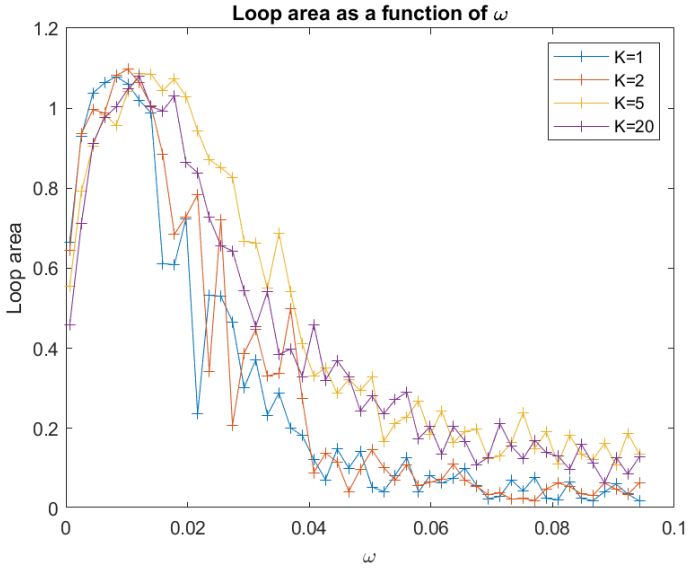

Figure 3.14: Loop area A as a function of the magnetic field's angular frequency ω

reached for a value of $\omega \sim 0.01$.

3.4 Convergence from the dynamic Ising model to the static one

3.4.1 Decreasing the magnetic field's amplitude B_0

When using a time-varying field, we can try to see how well it converges to the static case. Let us recover the dynamic critical temperatures for a given anisotropy by making the amplitude of the field B_0 closer to 0. In this case, we expect the values of the critical temperature, at fixed anisotropy factor, to get closer to the static case ($B = 0$) as the amplitude of the field decreases. The conditions are the same as in section 3.2, with $P = 1000$. We determine the critical temperature as previously, by looking at the dynamic order parameter and then cross-checking the estimate with the intersection of the BINDER cumulants, as the paper by SELKE [7] shows. We used different values for the amplitude, namely $B_0 \in \{0.1; 0.25; 0.5\}$ and plotted the graph $T_c = f(\alpha)$ for these four values, comparing these experimental curves with the analytical curve in the zero-field static case we already plotted in Fig. 3.6.

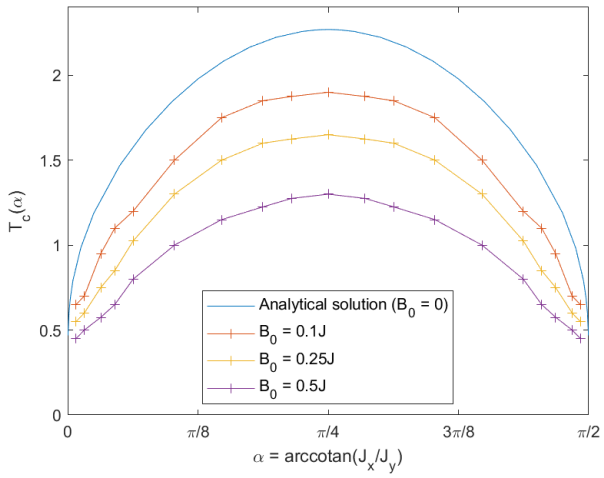

Figure 3.15: Evolution of the graph $T_c = f(\alpha)$ for different values of the amplitude B_0

We observe, as expected, that the curve $T_c = f(\alpha)$ is getting closer to the analytical one when the magnetic field is getting weaker. This effect is very marked for low anisotropies (in the center of Fig. 3.15, while it tends to get

weaker as we reach the edges of the graph. For example, for $K = 1$, the critical temperature passes from 2.27 in the ideal static case to 1.20 with an amplitude $B_0 = 0.5$ in the dynamic case. More generally, it seems that decreasing the magnetic field is an efficient method to recover the static limit by using the dynamic algorithm.

We also see that the curves converge towards a finite temperature (>0) when getting closer to the edges. The case $\alpha = 0$ corresponding to the 1D case, we would expect a zero dynamic critical temperature at this point. By running a real Monte-Carlo 1D algorithm (with the *Metropolis* dynamics), the dynamic critical temperature is extremely close to zero (Q is still zero for $T = 0.001$ by using this algorithm). By looking at the curves on Fig. 3.15, we could therefore reasonably conclude that the algorithm overestimates T_c for strong anisotropies (considering the two points closest to the edges here, where the curve is becoming less steep), that is below $\alpha = \frac{\pi}{32}$.

We can also try to recover a relationship for the decreasing factor of the critical temperature with respect to the amplitude of the magnetic field. Indeed, looking at Fig. 3.15, it seems that there might be some multiplicative factor $a(B_0)$ between the curves of the dynamic critical temperature $T_{c,B_0}(\alpha)$ and the ideal static curve in a zero-field configuration.

We apply the following steps to confirm this relationship : first, we perform a linear least square regression to estimate the best-fitting multiplicative factor $a^*(B_0)$ for given values of the magnetic field (here $B_0 \in \{0.1; 0.175; 0.25; 0.375; 0.5\}$). Three examples are shown on Fig. 3.16 (omitting the points at the edges for which the estimation given by the algorithm does not seem too good as mentioned above).

Table 3.1 lists the best-fitting multiplicative factors found for the amplitudes we consider.

When performing a linear regression of these two datasets, we obtain a fair correlation, with a determination coefficient $R^2 = 0.984$, yielding the graph in Fig. 3.17.

This linear correlation is very well verified for field amplitudes lower or equal than 0.5. If we try to plot the same curve as Fig. 3.15, but adding the dynamic critical temperatures when $B_0 = 0.7$ and $B_0 = 0.9$, we obtain the

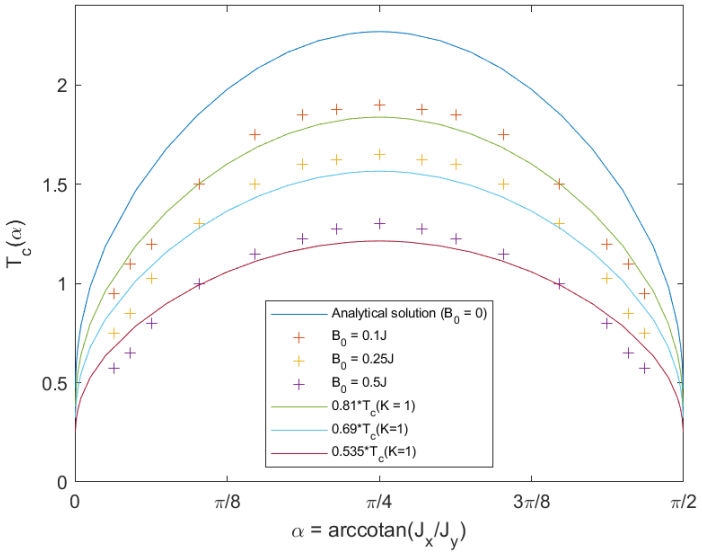

Figure 3.16: Evolution of the graph $T_c = f(\alpha)$ for different values of the amplitude B_0 with their best fitting curve $T_c = a^*(B_0)T_c(B_0 = 0)$ (solid line)

Field amplitude B_0	Best-fitting factor $a^*(B_0)$ (Resolution $\delta = 0.005$)
0.1	0.810
0.145	0.795
0.175	0.780
0.21	0.745
0.25	0.690
0.325	0.650
0.375	0.605
0.45	0.575
0.5	0.535

Table 3.1: Value of the best-fitting multiplicative factor for the estimation of $T_{c,B_0}(\alpha)$

curve shown in Fig. 3.18.

We observe that for $B_0 > 0.5J$ the curves become very flat in the edges when the anisotropy starts increasing. Therefore, the fitting would be not so adapted for the entire range of values of α we are considering. However, the central values (up to $\alpha \simeq 0.32$ approximately i.e. $K \simeq 3$) seem to be in compliance with a fitting $T_c(B_0) = a(B_0)T_c(B_0 = 0)$. Indeed, when performing a fitting of this form in this limited area ($K \in [1;3]$), we have a good correlation even for $B_0 > 0.5$. The linear regression between the best-fitting multiplicative factor $a^*(B_0)$ (over the restricted interval) and the magnetic field B_0 yields

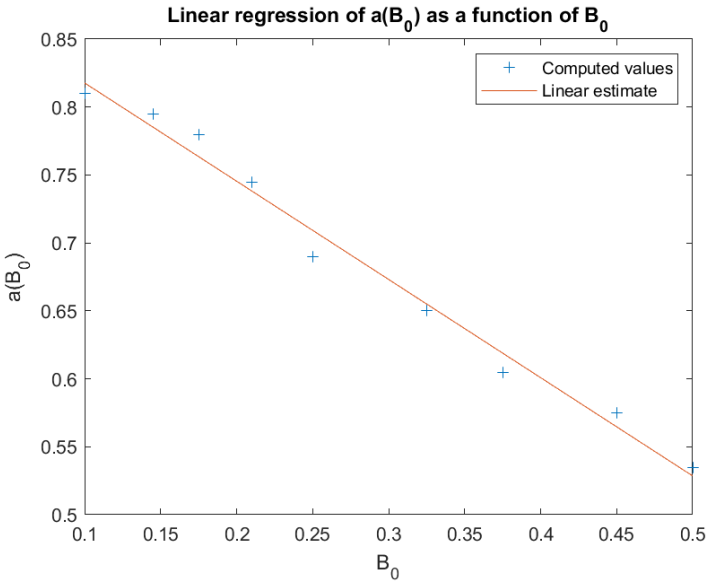

Figure 3.17: Linear regression $a^*(B_0) = f(B_0)$

also here a satisfying result, with a determination coefficient $R^2 = 0.985$.

3.4.2 Decreasing the period P

Another way we can think of in order to converge towards the static case would be to decrease the period of the magnetic field. Indeed, if the magnetic field is very slow (i.e. has a huge period like $P = 20000$), then the magnetization will be able even for lower temperatures to follow at least partially the magnetic field, as we can see on Fig. 3.19b : for some extrema of the field, the magnetization goes from one orientation to the other. However, for faster fields, with $P = 1000$, the magnetization for so low temperatures as $T = 1.3$ does not revert because the field is too fast, as shown on Fig. 3.19a. Therefore, at a given temperature, the order parameter will be higher for the configuration with a higher field cycle.

Let us try to see the evolution of the dynamic critical temperature with respect to the period P for different anisotropies. To determine the value of $T_c(P)$, we use the variance of the system $\mathcal{V} = L^2(\langle Q^2 \rangle - \langle |Q| \rangle^2)$ which presents a maximum for the critical temperature, with analogy to the magnetic susceptibility in the static case.

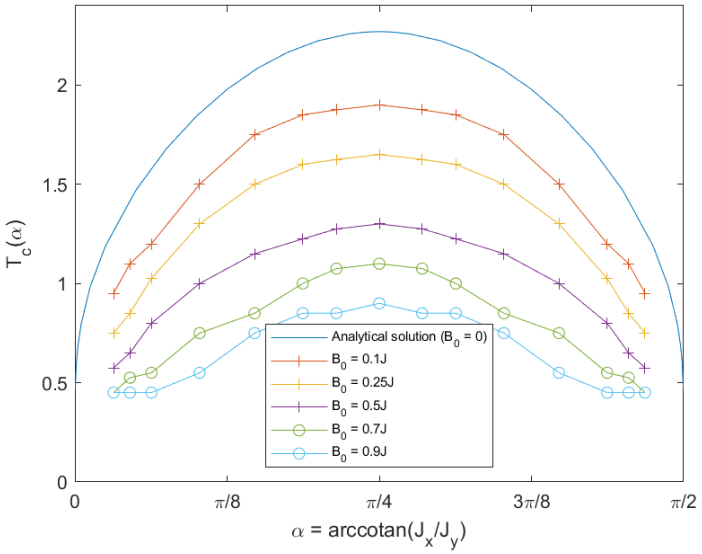

Figure 3.18: $T_c = f(\alpha)$ for various values of the field's amplitude B_0

We then apply a period sweep with equally spaced logarithmic values from 100 to 20000, so as to cover three different orders of magnitude) to see the evolution of the position of the peak for different anisotropies, using a 30×30 lattice and a temperature step of $\Delta T = 0.025$. The graph in Fig. 3.20 featuring the the evolution of the critical temperature as the period increases (the x-axis for P is rendered logarithmic so as to make the graph more regular), and as predicted, T_c diminishes when the period increases, for any anisotropy.

Let us try to guess an analytic behaviour for the curve in the isotropic case, so as to define reference values. Looking at the curve, a reasonable analytic formula able to fit well the data could be of the form :

$$T_{c_{K=1},\text{analytical}}(P) = \frac{a}{\log_{10}(P)} + b, \tag{3.4}$$

where a and b are two parameters to estimate. Performing the consequent linear regression, we obtain a very fair correlation with a determination coefficient $R^2 = 0.991$, the two ideal parameters being $(a^* = 2.682, b^* = 0.748)$. This is an Arrhenius-like behaviour, since we can write P in an exponential fashion and a can be considered as an activation energy term.

Interestingly, the curves have a very similar look. So as to fit them, we could think of a translating term ΔT_K such that for any given period P (in the range

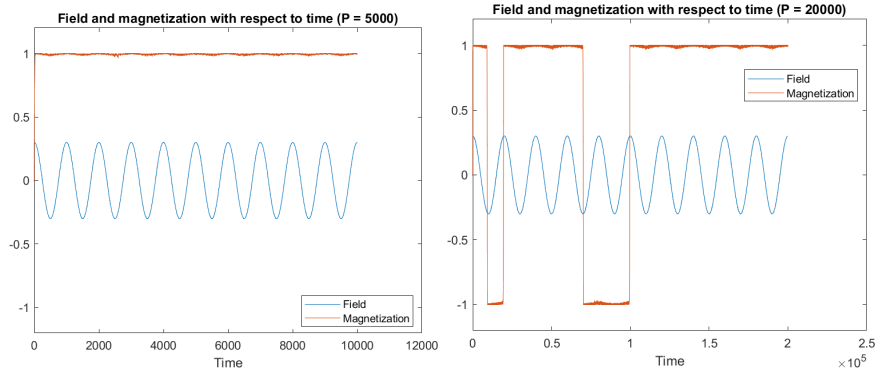

(a) $P = 1000$ **(b)** $P = 20000$

Figure 3.19: Temporal evolution of $B(t)$ and $M(t)$ over 10 periods for $K = 1$ and $T = 1.3$

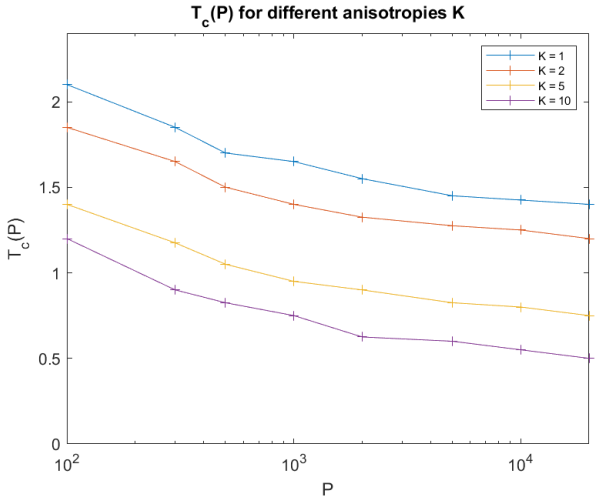

Figure 3.20: Plot of $T_c(P)$ for $K \in \{1; 2; 5; 10\}$

we consider), we have $T_{c_K} = T_{c_{K=1}} + \Delta T_K$, with $\Delta T_K < 0$.

We perform a linear least squares fitting between the actual values of the critical temperature we found thanks to the variance and the predicted behaviour, in order to find for a given anisotropy the additive term ΔT_K that minimizes best the sum :

$$\sum_{i=1}^{N_p} [T_{c_K}(P) - (T_{c_{K=1}}(P) + \Delta T_K)]^2, \tag{3.5}$$

where N_p is the number of different periods we consider. We apply this operation for all integer anisotropies between 2 and 10. The table 3.2 lists all

the values we found for the term ΔT_K when looking at anisotropies from 2 to 10.

Anisotropy factor K	Best-fitting term ΔT_K (Resolution $\delta T = 0.005$)
2	-0.210
3	-0.340
4	-0.425
5	-0.610
6	-0.590
7	-0.650
8	-0.740
9	-0.865
10	-0.895

Table 3.2: Value of the best-fitting additive term for the estimation of T

Fig. 3.21 shows an example of the superposition of the best fitting term and the actual critical temperature alongside the period. When performing a

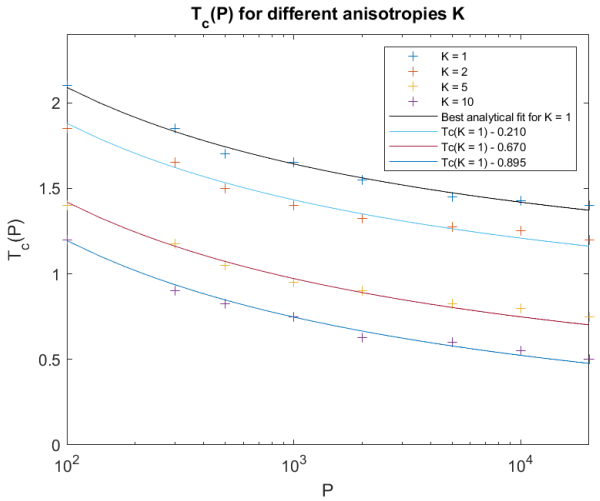

Figure 3.21: Plot of $T_c(P)$ for $K \in \{1; 2; 5; 10\}$, alongside with the best-fitting curves

linear regression of ΔK as a function of K, a pretty good result comes out, namely with a determination coefficient $R^2 = 0.93$, taking into account the fact that this value is strongly decreases by the not so good concordance for $K = 5$ (removing the data for $K = 5$, R^2 becomes 0.992). This linear fitting is shown in Fig. 3.22, with a slope $a = -0.082$ and an intercept $b = -0.11$ (this value being fairly consistant with the fact that we should ideally have a zero

value for ΔT_K at the origin). The activation factor a does not depend on the value K, only the additive b term does.

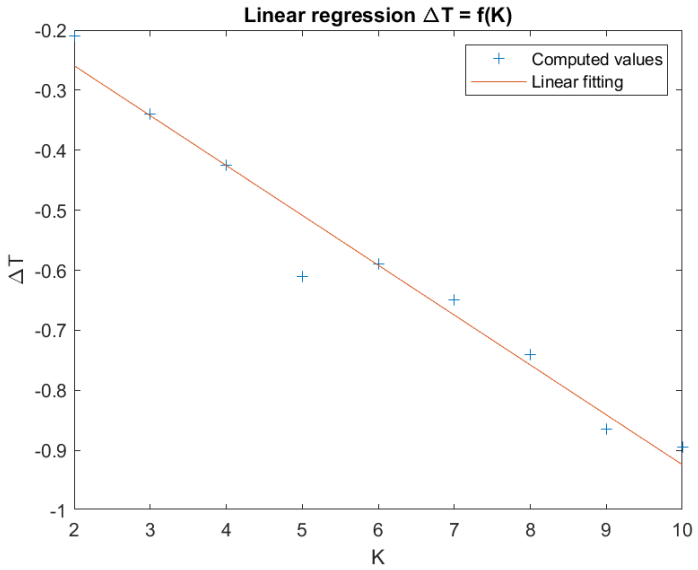

Figure 3.22: Linear fitting Δ

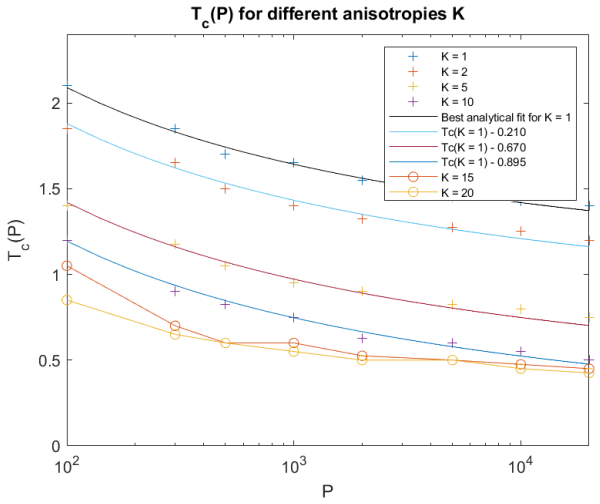

Figure 3.23: $T_c = f(P)$ with the cases $K = 15$ and $K = 20$

This relationship remains valid for a limited range of the anisotropy factor K. Indeed, when computing the dynamic critical temperatures with different periods of the magnetic field for $K = 15$ or $K = 20$, we obtain the graph shown in Fig. 3.23. The curves in these two cases have become very close and so the linear evolution of the translating term ΔT_K we highlighted for $K \leqslant 10$ is no longer present.

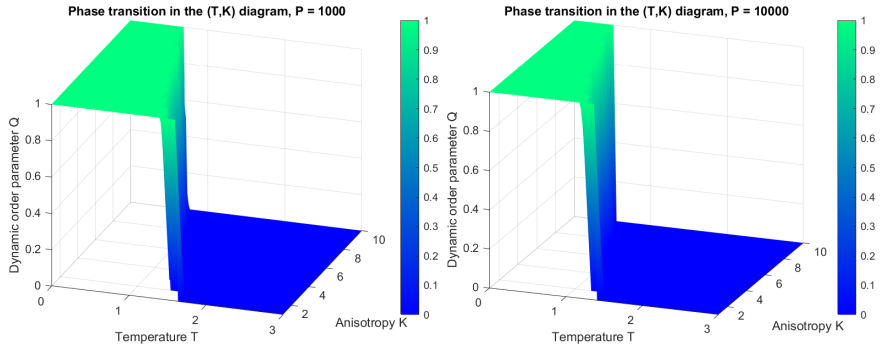

(a) $P = 1000$ **(b)** $P = 10000$

Figure 3.24: Phase transition diagram in the (T, K, Q) 3D space ($B_0 = 0.3$)

3.5 Phase diagrams

3.5.1 $T - K$ phase transition

Dynamic phase transitions, as we have seen, depend on many different variables. Let us now try to draw some 3D phase diagrams to better illustrate these phenomena. For example, if we fix the amplitude and the period of the external field, we are able to draw a diagram (T, K, Q) to show the limit between the dynamic ordered phase ($Q = 1$) and the dynamic disordered phase ($Q = 0$). For $B_0 = 0.3$, we drew the phase diagrams for the periods $P = 1000$ and $P = 10000$, that are shown in Fig. 3.24a and Fig. 3.24b. The number of cycles that we used is $N_p = 1000$ and we used a randomly distributed lattice as initial system.

Furthermore, we can project these 3D plots on the (T,K) plane so as to have a picture of the evolution of T_c along with these two variables, as it is shown on Fig. 3.25a and Fig. 3.25b. The linear trend that we observe for the critical temperature as a function of a the anisotropy factor seems to be confirmed here, for the range $1 \leqslant K \leqslant 10$. We also see that on the same diagram, the dynamic disordered phase occupies a higher surface for $P = 10000$, since the critical temperature, for any anisotropy, is lower than the one for $P = 1000$.

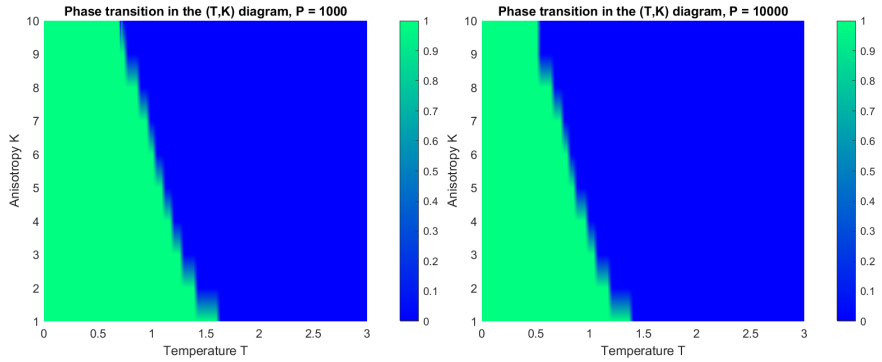

(a) $P = 1000$ **(b)** $P = 10000$

Figure 3.25: Phase transition diagram in the (T, K) 2D space ($B_0 = 0.3$)

3.5.2 $T - B_0$ phase transition

Changing our paradigm, we can plot phase diagrams in an other plane, that is the $T - B_0$ one, using this time the anisotropy factor as a parameter and fixing the period of the field ($P = 1000$). We get 3D plots of the disorder parameter as a function of both the temperature and the magnetic field's amplitude.

The effect of the anisotropy is clearly visible on how the green area is reduced when K increases. The border is shifted towards lower temperatures.

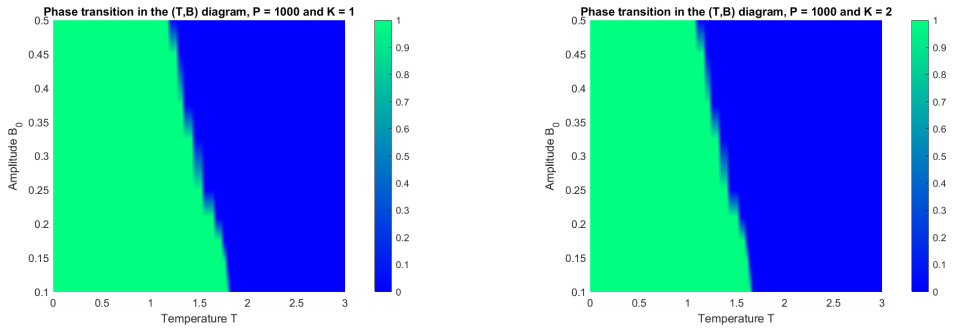

(a) $K = 1$ **(b)** $K = 2$

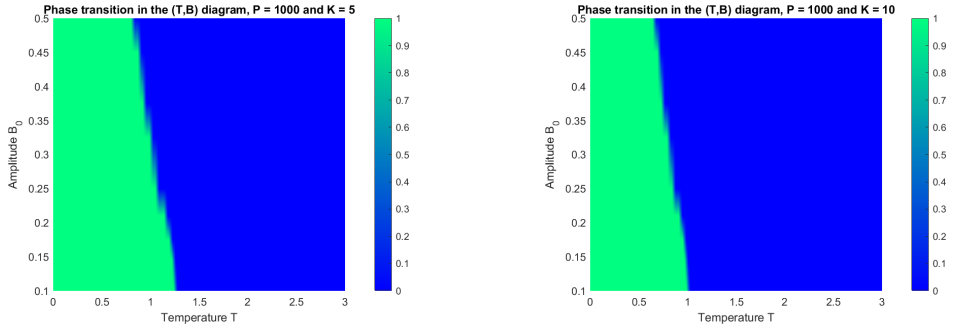

(c) $K = 5$ **(d)** $K = 10$

Figure 3.26: Phase transition diagrams $T - B_0$ for diverse anisotropies ($P = 1000$)

Chapter 4

Impact of randomness in the model

The lattices we have tackled so far were ideal spin lattices. Indeed, in real ferromagnets, the bonds between the spins J_x and J_y might not be the same all over the lattice. A possible way to simulate such a configuration is to introduce randomness in each bond of the lattice.

4.1 Random Anisotropy Ising Model (RAIM)

4.1.1 Theoretical frawework

The main idea for the Random-Bond Ising Model (shortened as RBIM) is to assume that the exchange interaction $J_{i,j}$ between a spin i and a spin j is variable, as written in Equation (4.1). In a classical isotropic spin lattice, we would assume a normal distribution and have the interaction parameter $J_{i,j}$ written in the following way :

$$f(J_{i,j}) = \frac{1}{\sqrt{2\pi R}} e^{-\frac{(J_{i,j}-\bar{J})^2}{2R}}, \tag{4.1}$$

where $\sqrt{R}$ is the standard deviation and $\bar{J}$ the mean of the gaussian distribution. R, comprised between 0 and 1, is also called the disorder parameter : when it is 0, there is no random component at all, i.e. the gaussian distribution becomes a DIRAC one, represented by a vertical straight line at the value $J_{i,j}$. Instead, when R increases, the gaussian curve becomes broader and broader.

However, within the anisotropic ISING model, we can not apply this formula in this way. Instead, we choose an approach that we could qualify of *Random Anisotropy Ising Model* (RAIM), where it is the anisotropy angle $\alpha = \text{arccotan}(K)$ which will bear the random component. Let us consider a lattice of (mean) anisotropy $\bar{K}$, we could calculate for each position in the lattice $(k, l) \in [\![1; L]\!] \times [\![1; L]\!]$ an anisotropy angle labeled as $\alpha_{k,l}$ according to the following distribution

$$g(\alpha_{k,l}) = \frac{1}{\sqrt{2\pi\sigma_\alpha(R)^2}} e^{-\frac{(\alpha_{k,l}-\bar{\alpha})^2}{2\sigma_\alpha(R)^2}}, \tag{4.2}$$

where the mean value of the distribution is the mean anisotropy angle $\bar{\alpha} = \text{arccotan}(\bar{K})$ and the standard deviation is $\sigma_\alpha(R)$, which will be derived later, so as to have scalable variation for different mean values of the anisotropy. Then, for each position of the lattice (k, l), we calculate the usual exchange coefficients J_x and J_y after fixing the value of J to 1 (following the relationship $\frac{J_x^2+J_y^2}{2} = 1$), as in the previous parts. The overall configuration will result in each spin of the lattice having its own interaction coefficient for its left and right neighbours $J_x(k, l)$ and its up and down neighbours $J_y(k, l)$. We deduce in the usual way the horizontal and vertical bonds for a given spin after choosing a random $\alpha_{k,l}$.

$$\begin{cases} J_x(k, l) = \sqrt{2}J\cos(\alpha_{k,l}); \\ J_y(k, l) = \sqrt{2}J\sin(\alpha_{k,l}). \end{cases} \tag{4.3}$$

Let us derive the optimal value for the standard deviation $\sigma_K(R)$, so as to have a scalable distribution for every value of the mean anisotropy. A good parameter to evaluate this is the probability of getting a negative anisotropy coefficient $P(\alpha_{k,l} < 0)$, given by the well-known formula below :

$$P_{\alpha_{k,l}<0} = \int_{-\infty}^{0} g(\alpha_{k,l})\, d\alpha_{k,l}. \tag{4.4}$$

By introducing the complementary error function $\text{erfc}(x) = \frac{2}{\sqrt{\pi}} \int_0^x e^{-t^2}\, dt$ and carrying out the following variable change $t = \frac{\bar{\alpha}-\alpha_{k,l}}{2\sigma_\alpha(R)}$, we can derive the following expression

$$P_{\alpha_{k,l}<0} = \frac{1}{2}\mathrm{erfc}\left(\frac{\bar{\alpha}}{2\sigma_\alpha(R)}\right). \tag{4.5}$$

As mentioned, we should have a *scalable* behaviour of this quantity. Therefore, the probability of "overflow" into the negative domain for the angle should not depend on the mean value of α ! Consequently, we must have, according to Eq. 4.5, $\sigma_\alpha(R) \propto \bar{\alpha}$. We can choose to introduce as the proportionality coefficient the square root of the disorder parameter $\sqrt{R}$.

Let us first visualize the gaussian distribution for the anisotropy angle α for several values of the disorder parameter R with a mean anisotropy angle of $\bar{\alpha} = \mathrm{arccotan}(\bar{K}) = 2$ and a standard deviation $\sigma_\alpha(R) = \bar{\alpha}\sqrt{R}$, i.e. $\bar{\alpha} = \mathrm{arccotan}(2) \sim 0.464$.

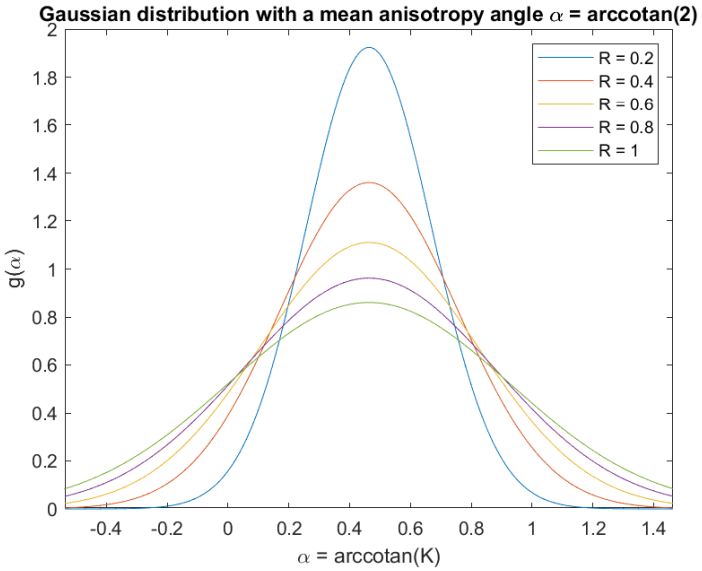

Figure 4.1: Normal distribution of the anisotropy ratio (here $\bar{\alpha} = \mathrm{arccotan}(2)$) for various values of $\sigma_\alpha = \bar{\alpha}\sqrt{R}$

We can see that there is a non-zero probability of getting a negative anisotropy angle. A crucial aspect in this distribution is therefore the way of handling the probability of getting a negative anisotropy angle $\alpha_{k,l} < 0$. This, according to Eq. 4.3 will lead to the bond in the vertical direction J_y changing sign and becoming negative, since sin is an odd function. J_x will remain unchanged because cos is an even function. Let us plot the proabability of getting a negative angle in a certain position (k, l) of the lattice as a function of the

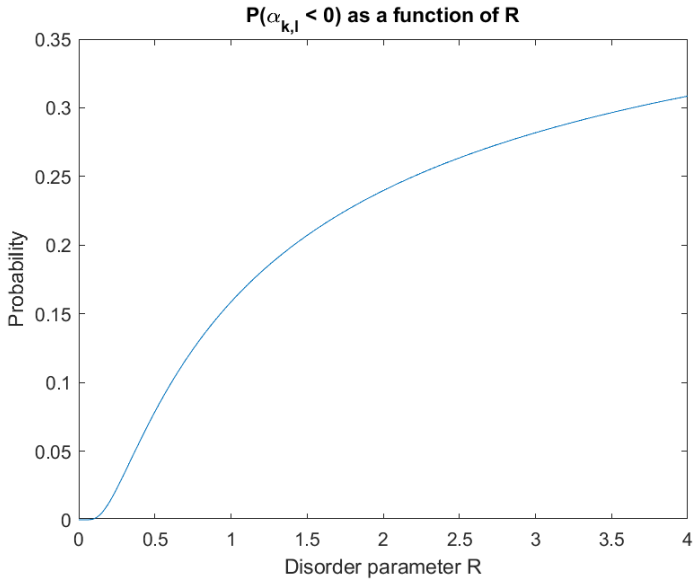

Figure 4.2: Probability of having a negative anisotropy angle $\alpha_{k,l}$ as a function of the disorder parameter R

disorder parameter R. According to what we did below, this probability is given by

$$P_R(\alpha_{k,l} < 0) = \frac{1}{2}\text{erfc}(\frac{1}{\sqrt{2R}}), \tag{4.6}$$

since it does not depend on the mean value of the anisotropy we consider. This curve has a shape shown on Fig. 4.2.

We must then fix a limit for the disorder parameter R_{max} until we can perform our computation so as to treat an actual ferromagnetic system. Indeed, if too many negative bonds are present, the physics of the system could change drastically. An estimate of the concentration in antiferromagnetic bonds (the ones for which $J < 0$, i.e. destroying the ferromagnetic order) has been found by N.K. JAGGI to be equal to 0.15, though some sources take it equal to 0.1. By precaution, we decide to fix the threshold to 0.1. Assuming that all spins are perfectly equivalent, i.e. that the proportion of antiferromagnetic bonds is equal to the probability of having a single spin of negative sign, we can recover the value of R_{max} we can treat.

We decide according to Fig. 4.3 to take as threshold $R_{max} = 0.6$. Not only this avoids considering possibly non-ferromagnetic systems, but it allows

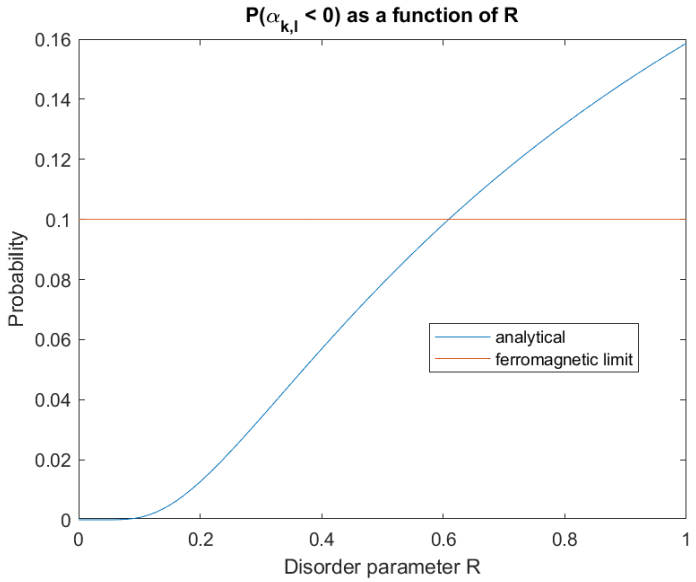

Figure 4.3: Probability of having a negative anisotropy factor $K_{k,l}$ with the ferromagnetic limit $P = 0.1$

to minimize the percentage of strange physical configurations, that is with classical positive bonds in the x-direction whereas the y-direction would allow negative bonds. Let us then detail how we introduced in practice the randomness into the model.

4.1.2 Implementation

Substantial changes to the algorithm must be made with respect to the one used in the previous parts, since a classes-like algorithm would not be suitable for the treatment of random anisotropy. Indeed, having randomly distributed bonds all over the lattice will make the number of classes possibly very large (18 times the number of spins in the lattice) : therefore, the treatment in the 18-fold way we applied so far becomes completely irrelevant, as it would make the simulation time explode. Therefore, we prefer the most classical version of the single spin-flip algorithm, that will be far more efficient. The dynamics is still the GLAUBER one, but instead of considering a probability rate per unit of time, we use an actual probability $p = \frac{1}{1+e^{-\frac{\Delta E}{k_B T}}}$, where $\Delta E = E_{old} - E_{new}$.

4.1.3 Evolution of the curves $T_c = f(\bar{\alpha})$ with R

We can now use the algorithm to calculate the magnetic susceptibility and deduce the critical temperature for a given value of the mean anisotropy angle $\bar{\alpha}$ and a given value of the disorder parameter. The plot presented in Fig. 4.4 represents the evolution of the plot $T_c = f(\bar{\alpha})$ for different values of the disorder parameter $R \in \{0.1; 0.2; 0.3; 0.5\}$, so as to have always a ferromagnetic behaviour of the lattice. We used a random initialization of the lattice and a decreasing temperature loop. We made 10 runs for each configuration, so as to compute in each case a mean value $\bar{T}_c$ and a standard deviation σ_{T_c} that account for the randomness of the system. The error bars show the interval $[\bar{T}_c - \sigma_{T_c}; \bar{T}_c + \sigma_{T_c}]$.

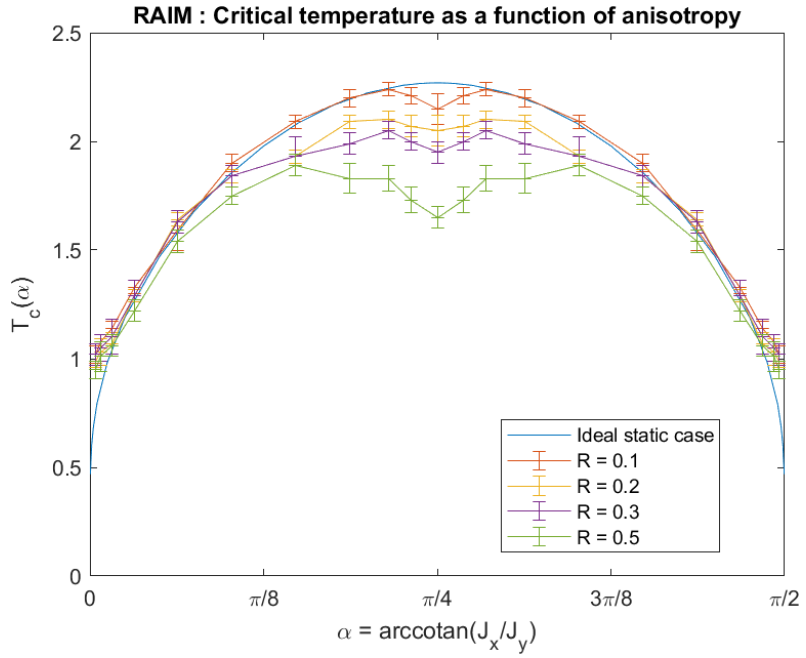

Figure 4.4: Plot of the critical temperature as a function of the mean anisotropy angle $\bar{\alpha}$ for different values of the disorder parameter

Several interesting observations can be made from this graph :

- the disorder parameter leads to a decrease in the critical temperature at all anisotropies. This was expected, since the fact of introducing a variation of the bond makes the lattice more similar to a 1D network, a configuration for which the critical temperature would converge to 0;

- unlike in the deterministic case, the maximum critical temperature is not reached for an on-average isotropic lattice ($\bar{\alpha} = \text{arccotan}(1)$), as we observe a slight decrease of T_c when getting closer to the center of the figure;
- the disorder parameter seems to have no effect when the anisotropy gets high, since the curves get superimposed for $\bar{\alpha} < 0.25$ (and on the other side, for $\bar{\alpha} > 1.35$).

The reason for the shifting of the maximum critical temperature towards anisotropies higher than can be explained in the following qualitative way : since we introduce a fluctuation of the anisotropy angle, the bonds in the lattice for a mean anisotropy angle $\bar{\alpha} = \frac{\pi}{4}$ will tend to assume values on average that are different from the perfectly isotropic case, which will lead to a decrease in the critical temperature. Instead, the slightly anisotropic mean angles will have a fair proportion of bonds that will be identical to the isotropic case. The position of the maximum is consequently shifted towards the left of the graph (i.e. lower anisotropy angles) when the disorder parameter decreases, since this leads to higher fluctuations of the mean anisotropy angle.

Why does the effect of the anisotropy get a higher weight than the disorder parameter as the mean value of the anisotropy factor increases ? So as to have a scalable behaviour of the system for different mean values of the anisotropies, the relative fluctuation was chosen identical (with $\sigma_\alpha = \sqrt{R}\bar{\alpha}$). This leads to a decreasing absolute fluctuation as the anisotropy increases (i.e. as the anisotropy angles decreases). So as to make an example, we can plot the function $g(K) = \text{arccotan}(2K) - \text{arccotan}(K)$. This quantity is a picture of how the fluctuation between a mean anisotropy angle and its double (hence separated by some number of standard deviations) goes with the value of the anisotropy factor. We observe that the randomness gets negligible as the system becomes more anisotropic, as Fig. 4.5 shows. In the center, for isotropic and weakly anisotropic lattices, the fluctuation is maximum between the angle corresponding to an anisotropy factor and the one corresponding to its double.

Furthermore, the overlapping curves for high anisotropies (i.e. for $\bar{\alpha} < 0.25$

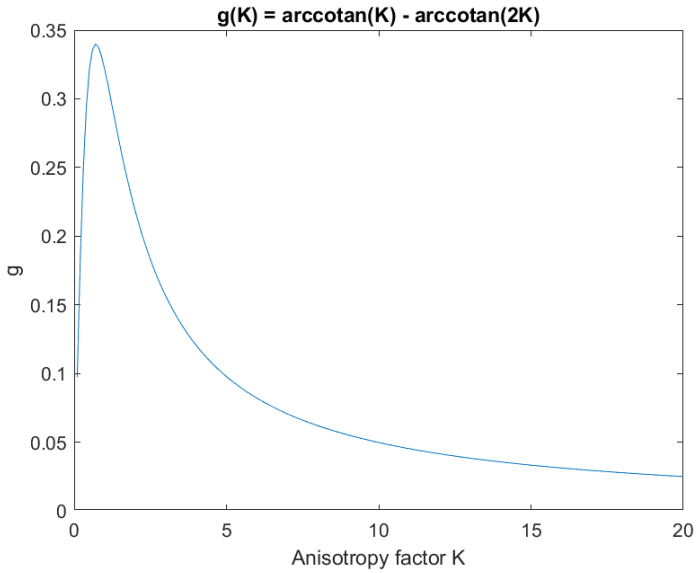

Figure 4.5: Fluctuation of the anisotropy angle with respect to the anisotropy factor

and for $\bar{\alpha} > 1.35$) can be interpolated pretty well by a linear trend, as can be seen on Fig. 4.6. The coefficients for the best fitting (based on the mean points of the four curves for a given $\bar{\alpha}$) are a slope $a = 3.26$ and a crossing $b = 0.95$.

In order to check that the physics of the system actually changes for disorder parameters higher than $R = 0.6$, let us plot the graph $T_c = f(\bar{\alpha})$ for the parameters $R = 0.8$ and $R = 1$, as shown in Fig. 4.7. This is clear that the shape has changed, with a very sharp peak in the center and a distinct decrease for larger anisotropies. As mentioned, these physical systems are tough to apprehend, as they are still ferromagnetic in one direction (the one corresponding to the cosine of the anisotropy angle), while the other direction will tend to have some negative bonds, making the different rows of the lattice trying to oppose each others. The temperatures plotted in this graph have still been determined with the position of the peak of the magnetic susceptibility. However, the expected behaviour of this quantity is not known in the case of a ferromagnetic lattice in one direction (the one for which the sign of the angle does not count) and of a spin glass in the other. Therefore, this nuances the reliability of the curves, that anyway show a behaviour that is different from the ferromagnetic case.

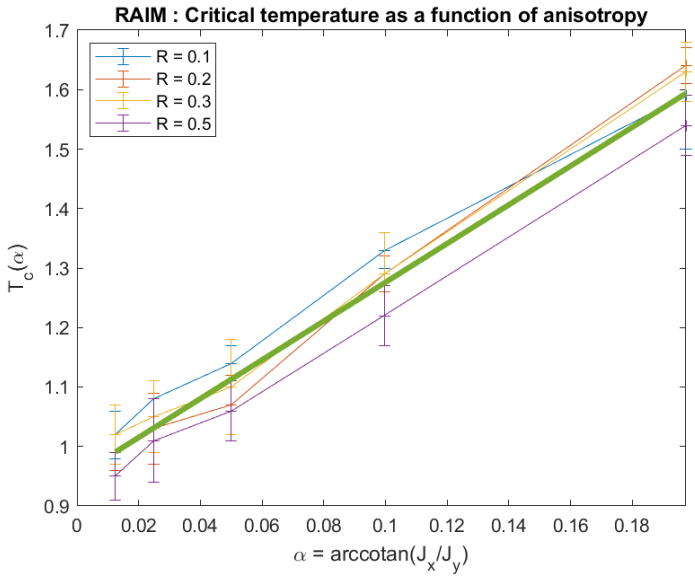

Figure 4.6: Linear trend for very high anisotropies

4.2 Fluctuation of the magnetization under the effect of a time-varying field

4.2.1 Impact of the anisotropy on the magnetization's noise

The noise of the magnetization has been tackled in diverse contexts. For example, PUPPIN and ZANI [11] studied the impact of the random-field Ising model. In Chapter 3, we saw the effect of the magnetic field's period on the dynamic critical temperature. We now want to investigate another aspect of the randomness in the behaviour of anisotropic spin lattices, namely the temperature fluctuation. If the temperature is below the dynamic critical temperature, the system is in the ordered phase. However, for temperatures very close to the transition temperature, typically $0.9T_c$, the magnetization becomes able to follow partially the magnetic field as we will see. Let us study the influence of the anisotropy factor on the magnetization's fluctuations at a typical subcritical temperature as $T = 0.9T_c$.

We choose a magnetic field's period $P = 1000$ (with amplitude $B_0 = 0.3$ as before). The figure Fig. 4.8 shows plots of the both the magnetic field and the magnetization for anisotropies $K = 1$, $K = 2$, $K = 5$ and $K = 10$, running the simulations for a total time **TimeMax** $= 200P$. The anisotropy acts as a

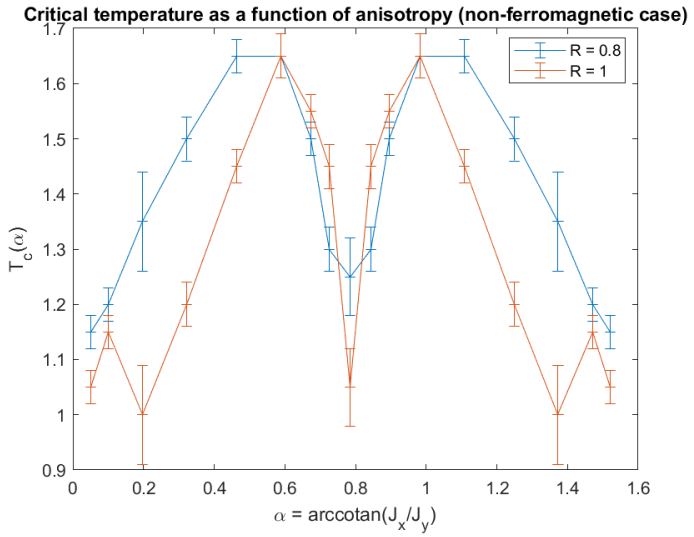

Figure 4.7: Critical temperature as a function of the mean anisotropy angle for $R = 0.8$ and $R = 1$

disorder agent : for $K = 1$ the magnetization is strongly located at $+1$, with the peaks symbolizing partial reversals of the magnetization as we see on Fig. 4.8a. When increasing K, the magnetization becomes more and more noisy, to the point that in Fig. 4.8d, the system does not oscillate anymore between -1 and +1 but is comprised in a smaller interval. We can also see that the attempted reversals are much more frequent when the anisotropy increases since they look much denser on the graphs in Fig. 4.8c and Fig. 4.8d than on plots in Fig. 4.8a and 4.8b.

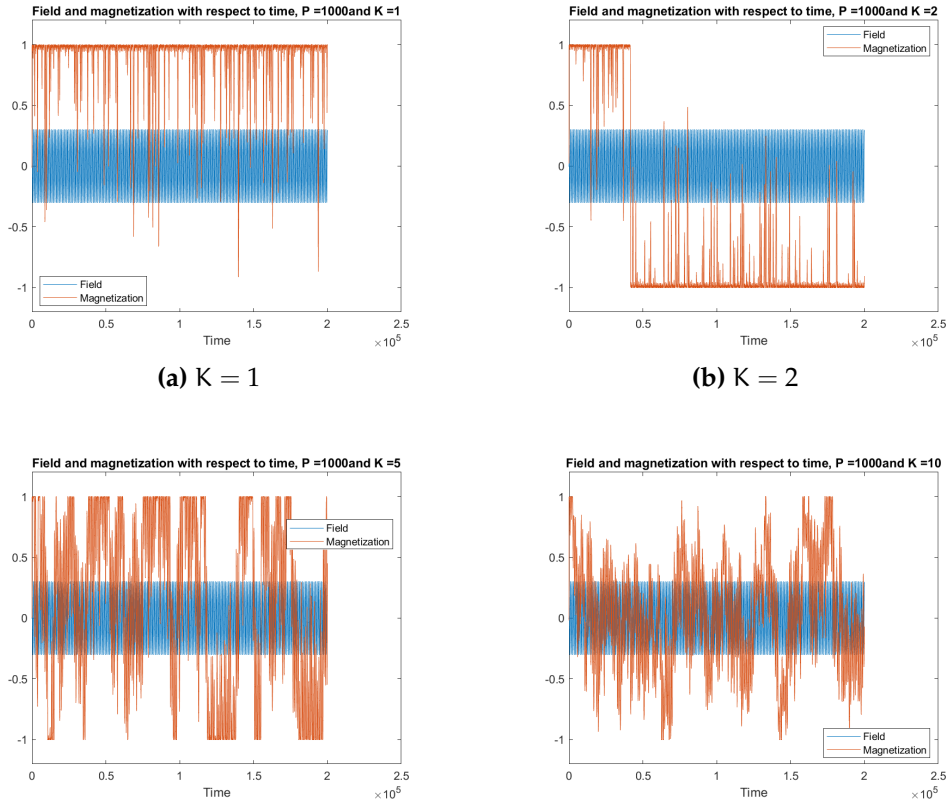

(a) K = 1 **(b)** K = 2

(c) K = 5 **(d)** K = 10

Figure 4.8: Magnetization and magnetic field along time for subcritical temperature $T = 0.9T_c$

4.2.2 Thermal excitation as a function of the anisotropy

To measure to what extent the magnetization is impacted by the temperature, i.e. the thermal excitation, we can define two thresholds :

- the temperature T_f of the first fluctuation, for which the ferromagnetic phase undergoes a first slight perturbation. A slight perturbation is defined as an attempted reversal with a jump equal to more than 0.05 (i.e. going at least from 1 to 0.95 or from -1 to -0.95);
- the temperature T_r of the first reversal, for which the magnetization experiences its first *complete* reversal, still in the ferromagnetic phase. We choose a duration of 50P, which is an arbitrary choice, but that seems reasonable to observe long-term phenomena such as reversals of the magnetization.

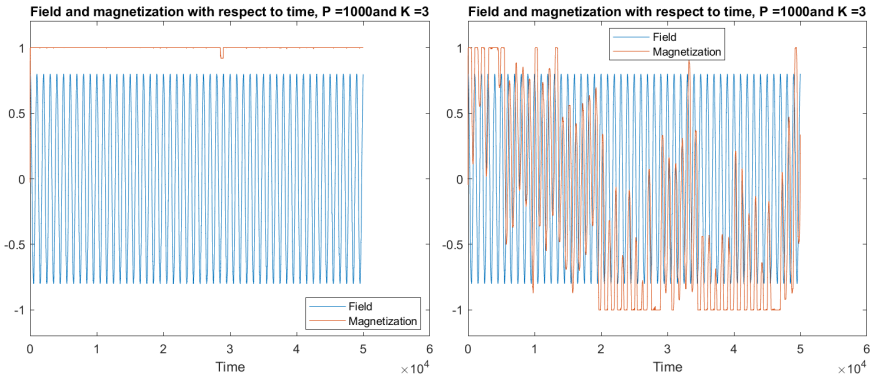

(a) First fluctuation **(b)** First reversal

Figure 4.9: First fluctuation and first reversal of the magnetization for $K = 3$ and $B_0 = 0.8$

These two thresholds are illustrated respectively on Fig. 4.9a and on Fig. 4.9b. We computed these temperatures for values of the field pertaining to $\{0.2; 0.4; 0.6; 0.8; 1\}$ and for an anisotropy factor $K \in \{1; 2; 3; 5\}$. The results are shown on Fig. 4.10. Since they are by definition arbitrary (in particular the threshold used for the first reversal and the duration of the experiment), we should repeat the experiment several times in order to have an estimate of the variation between measurements under the same conditions. Furthemore, they are defined for a given dimension of the lattice, $L = 50$. Changing the size of the system might result as well in some variations.

As expected, we observe a decrease of the fluctuation and the reversal temperatures for a fixed field's value when the anisotropy increases and for a fixed anisotropy when the field increases. Furthermore, we notice that there is a clear difference between the isotropic case and the anisotropic ones (for $K = 2, 3$ and 5), since the two temperatures are almost the same in the case of an isotropic configuration, whereas the anisotropic configurations clearly exhibit a significant gap between T_f and T_r, that we can estimate around $0.2\frac{J}{k_B}$ on average. Qualitatively, this means that the thermal excitation is active on a broader range for anisotropic lattices.

We notice that the curve of the first reversal temperature is getting closer to the critical one as the anisotropy increases. This is confirmed by calculating the sum of the square errors between the two curves. For the total subcritical excitation (the difference between the critical curve and the one for the first

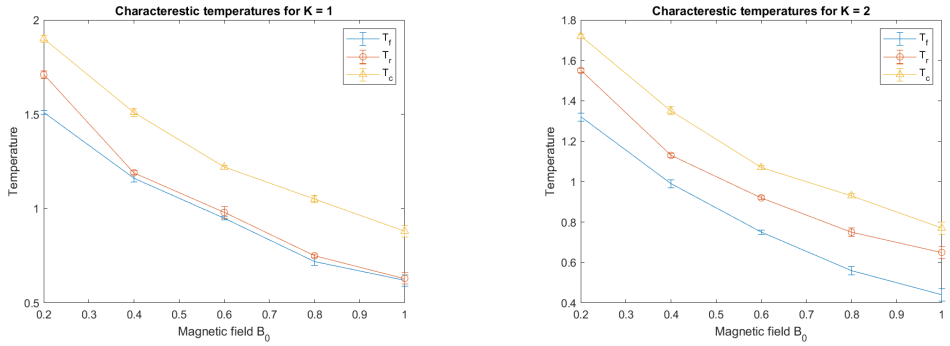

(a) K = 1

(b) K = 2

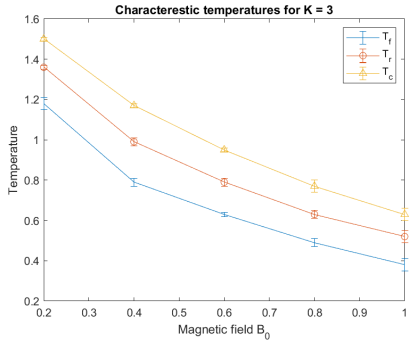

(c) K = 3

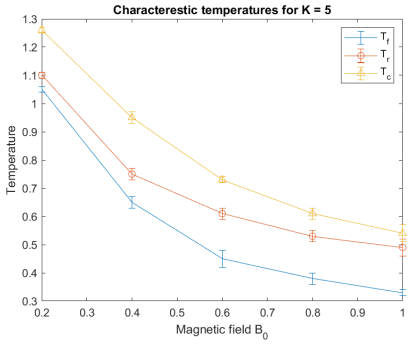

(d) K = 5

Figure 4.10: Magnetization and magnetic field along time for subcritical temperature $T = 0.9T_c$

fluctuation) instead, a maximum is observed for K = 2.

Of course, a more quantitative analysis would be hard to perform given the number of independent parameters : the dimension of the lattice, the period of the field (in this case P = 1000), the mesh for the amplitude of the field...). Doubling the size of the lattice yields however very similar results.

Chapter 5

Anisotropy and dimensionality of the lattice

Finally, we can investigate the transition from a one-dimensional spin chain towards a 2D isotropic lattice, in order to determine how the critical temperature goes from zero to a finite value as the anisotropy becomes weaker. The implemented system is a 10000×4 chain as shown in Fig. 5.1. We start

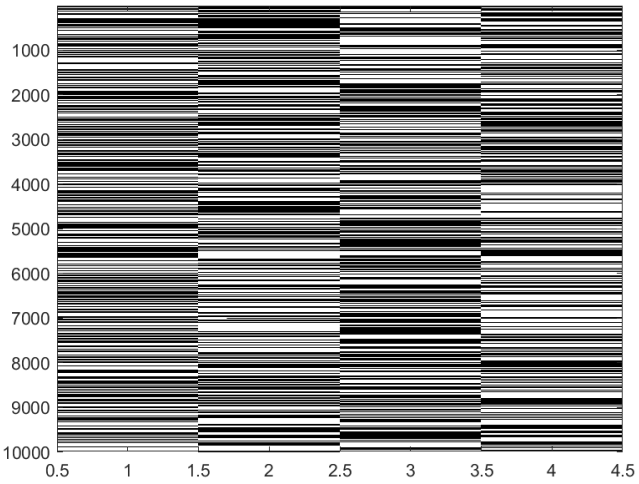

Figure 5.1: A 10000×4 spin lattice with $\frac{J_x}{J_y} = 10^{-2}$

verifying that no phase transition is observed for the case $J_x = 0$, when the lattice is only made of non-correlated 1D stripes. Then, we start increasing the exchange interaction constant between these stripes, in order to simulate the transition from a 1D lattice into a 2D one. We obtain the graph presented

in Fig. 5.2. From this graph, it appears that there is a change of behaviour

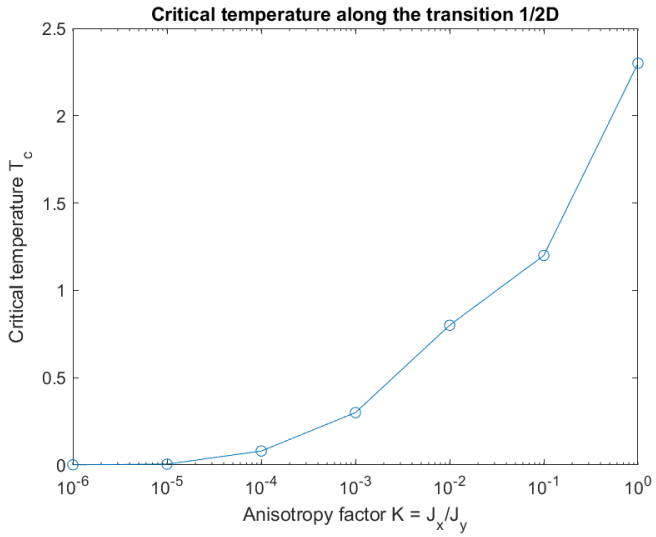

Figure 5.2: Increase of T_c as the material gets two-dimensional

from $K = 10^{-4}$, since above this value, the critical temperature is getting high, while it remains very close to 0 for stronger anisotropies : $T_c = 0.001$ for $K = 10^{-6}$ and $T_c = 0.005$ for $K = 10^{-5}$. Furthermore, this curve is coherent with the analytical expectation by Onsager presented in Fig. 2.12, plotting it in a semi-logarithmic way.

In 1992, NOVOTNY [16] plotted the critical temperature of a lattice of dimension d comprised between 1 and 2 (non-integer values were obtained thanks to interpolation). By fitting the values he obtained with the analytical prediction of ONSAGER, we can plot the dimensionality of the lattice as a function of the anisotropy factor K. Fig. 5.3 shows this graph.

We observe that there is a very strong decrease of the dimensionality occurring for quite low values of $K \leqslant 5$. However, once $d \sim 1.1$ is reached, the decrease becomes extremely slow and progressive and the true one-dimensional lattice will be reached only at the limit of an infinitely anisotropic lattice. This is coherent with the fact that we observe still a finite critical temperature even when the anisotropy constant is very low.

The link between the anisotropy and the dimensionality is however not so simple to deduce. Indeed, in the same article, NOVOTNY plotted the relationship between the inverse of the critical exponent ν (appearing in the expression

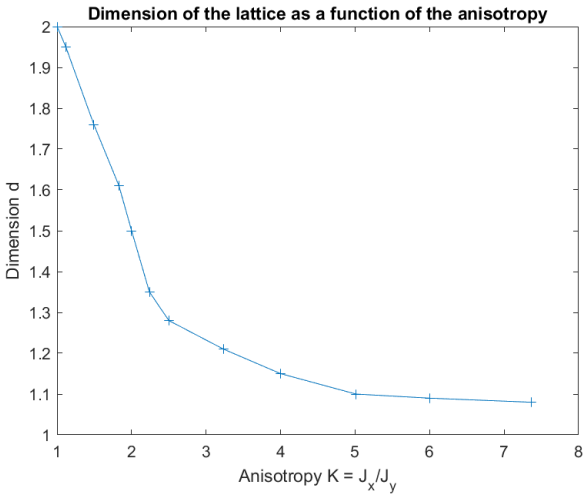

Figure 5.3: Estimated dimensionality of the lattice as a function of the anisotropy factor (based on the values of T_c)

of the correlation length $\xi = \left|\frac{T-T_c}{T_c}\right|^{-\nu}$) and the lattice dimensionality d, as shown on Fig. 5.4.

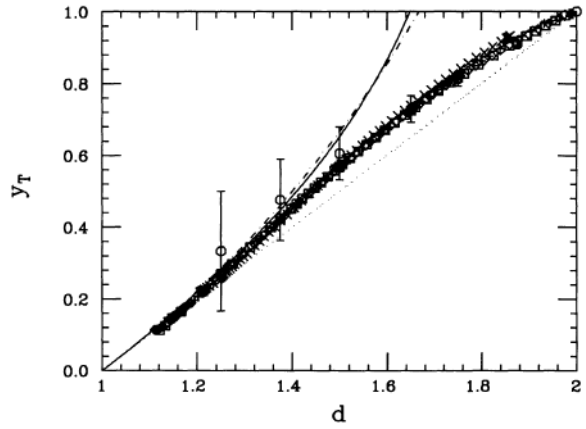

Figure 5.4: $y_T = \frac{1}{\nu}$ as a function of the lattice's dimensionality (NOVOTNY, [16])

We notice a clear variation of the critical exponent when d goes from 2 to 1. However, when computing the critical exponent with our algorithm for different anisotropies, using the scaling equation given in the book by BINDER and LANDAU [4], we always obtain a value of ν around 1, which is also confirmed by the works of FARSAL [14]. Therefore, we can not state that there is a direct equivalency the concepts of anisotropy and dimensionality.

Conclusions and future developments

To wrap up, the original results of this thesis are multiple :

1. the impact of a time-varying sinusoidal magnetic field (its amplitude and its period) on an anisotropic spin lattice;
2. the elaboration of multiple three-dimensional phase diagrams for the dynamic order parameter as a function of diverse quantities (the anisotropy factor K, the period P and the amplitude B_0);
3. the introduction of the Random-Anisotropy Ising Model to study the impact of randomness in an anisotropic spin lattice.

In the first point, our calculations showed that the critical temperature is decreasing, on one hand when the field's amplitude becomes higher for a fixed period, and on the other hand, when the field's period becomes smaller for a fixed amplitude. We extrapolated trends of these evolutions as a function of the anisotropy, showed on Fig. a. and Fig. b.

We then obtained various phase diagrams for the dynamic order parameter between the dynamic ordered phase ($Q = 1$ in green) and the dynamic disordered phase ($Q = 0$ in blue). Fig. ca and Fig. cb show the (T, K, Q) diagrams for various values of the period for example. This allowed to notice a linear effect of the anisotropy (up to $K = 10$) on the decrease of the dynamic critical temperature.

Finally, we implemented, by analogy with the Random-Bond Ising Model, the Random-Anisotropy Model, that is based on a gaussian distribution of

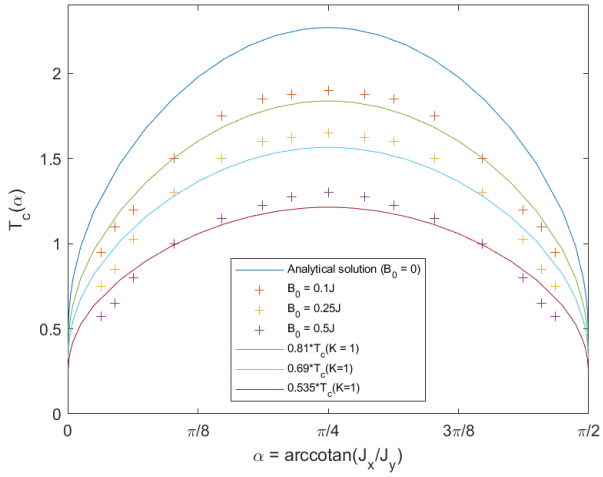

Figure a: Evolution of the graph $T_c = f(\alpha)$ for different values of the amplitude B_0 with their best-fitting curve $T_c = a^*(B_0)T_c(B_0 = 0)$ (solid line)

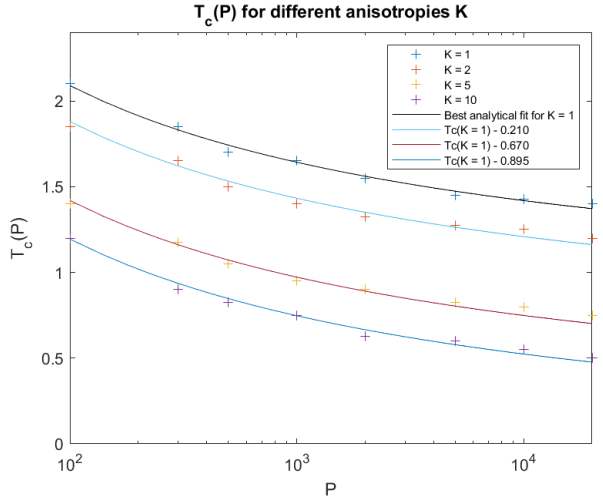

Figure b: Plot of $T_c(P)$ for $K \in \{1; 2; 5; 10\}$, alongside with the best-fitting curves

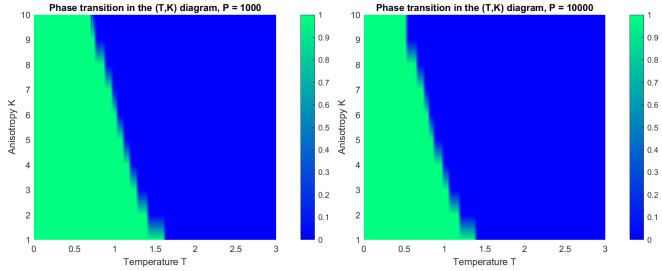

(a) $P = 1000$ **(b)** $P = 10000$

Figure c: Phase transition diagram in the (T, K) 2D space ($B_0 = 0.3$)

the anisotropy. After verifying the conditions for which the material can still be considered ferromagnetic, we launched several simulations for various values of the disorder parameter R and various values of the mean anisotropy angle $\bar{\alpha}$. We obtained the graph shown in Fig. d.

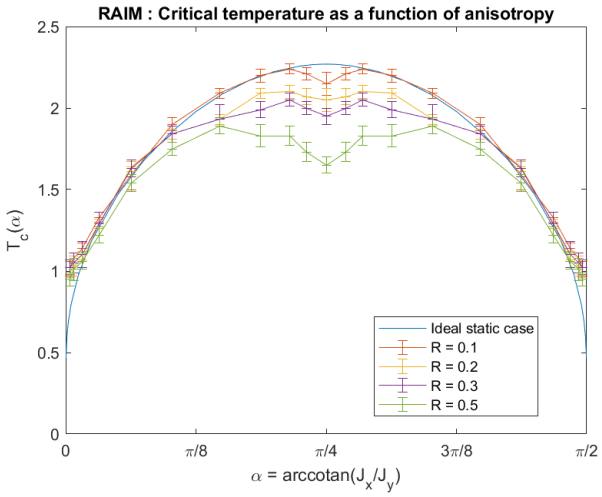

Figure d: Plot of the critical temperature as a function of the mean anisotropy angle $\bar{\alpha}$ for different values of the disorder parameter

From the computational point of view, a future perspective would be to write the dynamic algorithm in a parallel way instead of the classical sequential method. Indeed, this would allow to treat way bigger lattices while keeping a small computation time. The idea is to divide the lattice into several regions that are treated by the various processors of the computer that is used for the simulation. This would be more difficult to implement, since each sublattice would have its own computational time and the management of the spin flips at the boundary between two domains have to be treated carefully.

Bibliography

1. M.E.J. NEWMAN and G.T. BARKEMA, *Monte Carlo Methods in Statistical Physics*, 1999;

2. A.B. BORTZ, M.H. KALOS and J.L. LEBOWITZ, *A New Monte Algorithm for Monte Carlo Simulation of Ising Spin Systems*, *Journal of Computational Physics 17*, 1975;

3. M.A. NOVOTNY, *A new approach to an old algorithm for the simulation of Ising-like Systems*, *Computers in Physics 9, 46*, 1995;

4. D.P. LANDAU and K. BINDER, *A guide to Monte Carlo Simulations in Statistical Physics*, 1999;

5. H.E. STANLEY, *Introduction to Phase Transitions and Critical Phenomena*, 1971;

6. W. SELKE and L.N. SHCHUR, *Critical Binder cumulant in two-dimensional anisotropic Ising models*, *J. Phys. A: Math. Gen. 38 L739–L744*, 2005;

7. L. ONSAGER, *A Two-Dimensional Model with an Order-Disorder Transition*, *Phys. Rev. Vol. 65*, 1944;

8. B.K. CHAKRABARTI AND M. ACHARYYA, *Dynamic transitions and hysteresis*, Reviews of Modern Physics, Vol. 71, No. 3, 1999;

9. Y. YÜKSEL AND E. VATANSEVER, *Dynamic phase transitions in classical Ising models*, J. Phys. D: Appl. Phys. 55 07300, 2022;

10. F. PERANI, *Cluster Monte-Carlo for Random-Bond Ising Model*, 2021;

11. L. CALLEGARO, E. PUPPIN AND M. ZANI, *Barkhausen jumps and metastability*, J. Phys. D: Appl. Phys. 36 2036–2040, 2003;

12. L. IMENEO, *Simulating the scaling function of the magnetic susceptibility for the 3D Heisenberg ferromagnet in tetragonal lattices*, 2021;

13. M. GHAEMI, M. GHANNADI, and B. MIRZA, *Calculation of The Critical Temperature for Anisotropic Two-Layer Ising Model Using The Transfer Matrix Method*, J. Phys. Chem. B, 107, 829-831, 2003;

14. D. FARSAL, M. SNINA, M. BADIA and M. BENNAI, *Critical Properties of Two-dimensional Anisotropic Ising Model on a Square Lattice*, J Supercond Nov Magn 0:2187–2195, 2017;

15. A. K. MURTAZAEVA and ZH. G. IBAEVA, *Thermodynamic and Magnetic Properties of the Two-Dimensional Anisotropic Ising Model with Competing Interactions*, Physics of the Solid State, Vol. 61, No. 10, 2019;

16. M. A. NOVOTNY, *Critical exponents for the Ising model between one and two dimensions*, Phys. Review B, Vol. 46, No 5, 1992;

17. J. L. LEBOWITZ,*A New Algorithm for Monte Carlo Simulations of Ising Spin Systems*, Journal of Computational Physics, Vol. 17, 1975.

List of Figures

List of Tables

Appendix : MATLAB code of the dynamic algorithm for an anisotropic Ising lattice

Listing 5.1: MATLAB Function **dynamic_anisotropic.m** used for the temporal evolution of a 2D anisotropic spin lattice

```
function [Energy,Magnetization,Magnetization2,Magnetization4,
   time,Lattice,Field,Energy2,contat] = dynamic_anisotropic(L,D
   ,T,Bb,Bzero,P,NofIter,Lattice,show,TimeMax,K)

    % Initialization of variables
    N = L^D; % Total number of spins
    NumClass = 18; % Number of classes of the system
    J = 1;
    % Variables of the system
    Kb = 1;
    beta = 1/(T*Kb); % Statistical temperature
    phi = acot(K); % Anisotropy angle
    Jx = sqrt(2)*J*cos(phi);  % Horizontal exchange
       interaction
    Jy = sqrt(2)*J*sin(phi); % Vertical exchange interaction
    muB = 1; %In terms of Hamiltonian we should consider muB*B
    timePause = 0.25;
    alph = 1; % Inverse of time used in the transition rate
       for each class

    % Variables as support
```

```
nArray = zeros(1,NumClass); % Number of spins in the class
    i
mArray = zeros(1,NumClass); % Keeps track of the number of
    spins with class lower than i
qArray = zeros(1,NumClass); % Array of the coefficient Q

% Initialization of the variables

Class = zeros(18,N); %list of the spin lattice by class
Location = zeros(L,L); %keeps track of the location inside
    class of each spin
Energy = [];
Magnetization = [];
time = [];
Field = [];

for i=1:L
    for j=1:L
        % Control the nearest neighbours
        contav = 0; % Counts spin up in vertical direction
        contah = 0; % Counts spins up in horizontal
           direction
        if(Lattice(mod(i,L)+1,j)==1)
            contah = contah +1;
        end
        if(Lattice(i,mod(j,L)+1)==1)
            contav = contav +1;
        end
        if(Lattice(mod(i-2,L)+1,j)==1)
            contah = contah +1;
        end
        if(Lattice(i,mod(j-2,L)+1)==1)
            contav = contav +1;
        end
        conta = contah + contav;
        if Lattice(i,j)==1
```

```
        % Class from 1 to 9 (Novotny classification,
           1995 article)
        if contah==2
            nArray(5 - conta) = nArray(5 - conta) + 1;
            Class(5-conta,nArray(5 -conta)) = i*18*L +
                j;
            for k=6-conta:NumClass
                mArray(k) = mArray(k)+1;
            end
        elseif contah == 1
            nArray(7 - conta) = nArray(7 - conta) + 1;
            Class(7-conta,nArray(7 -conta)) = i*18*L +
                j;
            for k=8-conta:NumClass
                mArray(k) = mArray(k)+1;
            end
        elseif contah == 0
            nArray(9 - conta) = nArray(9 - conta) + 1;
            Class(9-conta,nArray(9 -conta)) = i*18*L +
                j;
            for k=10-conta:NumClass
                mArray(k) = mArray(k)+1;
            end
        end
    else
        % Class from 10 to 18 (Novotny classification,
            1995 article)

        if contah==2
            nArray(14 - conta) = nArray(14 - conta) +
               1;
            Class(14-conta,nArray(14 -conta)) = i*18*L
                + j;
            for k=15-conta:NumClass
                mArray(k) = mArray(k)+1;
            end
```

```
            elseif contah == 1
                nArray(16 - conta) = nArray(16 - conta) +
                   1;
                Class(16-conta,nArray(16 -conta)) = i*18*L
                    + j;
                for k=17-conta:NumClass
                    mArray(k) = mArray(k)+1;
                end
            elseif contah == 0
                nArray(18 - conta) = nArray(18 - conta) +
                   1;
                Class(18-conta,nArray(18 -conta)) = i*18*L
                    + j;
                for k=19-conta:NumClass
                    mArray(k) = mArray(k)+1;
                end
            end
        end

    end
end

% Update Location matrix
for j=1:NumClass
    for i=1:N
        if (Class(j,i)~=0)
            Location(floor(Class(j,i)/(L*18)),mod(Class(j,
               i),L*18)) = 18*18*i+j;
        end
    end
end

% Calculation of energy and magnetization
Magnetization(1) = sum(sum(Lattice))/N;
Magnetization2(1) = Magnetization(1)^2;
Magnetization4(1) = Magnetization(1)^4;
```

```
Energy(1) = 0;
for i=1:L
    for j=1:L
        Energy(1) = Energy(1) - Jx*Lattice(i,j)*Lattice(
           mod(i,L)+1,j)/N - Jy*Lattice(i,j)*Lattice(i,mod(
           j,L)+1)/N-(Bb+Bzero)*Lattice(i,j)/N;
    end
end

if show == 1
    figure(1)
    imagesc(mod(Location,18*18),[-1 18]);
    colormap(hot(256))
    title('Class');
    figure(2)
    imagesc(Lattice);
    colormap(hot(256))
    title('Lattice');
    drawnow
    pause(timePause);
end

t = 1;

tempP = 0;
time(1) = 0;
Field(1) = 0;

% Actual Kinetic MonteCarlo
while time(t)<TimeMax

    % Determination of the new transition probabilities
    B = Bb + Bzero*cos(2*pi/P*time(t));

    % Novotny
    ClassEnergy = Jx*[2 2 2 0 0 0 -2 -2 -2 -2 -2 -2 0 0 0
```

```
   2 2 2] + Jy*[2 0 -2 2 0 -2 2 0 -2 -2 0 2 -2 0 2 -2 0
    2] - abs(Field(t))*muB*[1 1 1 1 1 1 1 1 1 -1 -1 -1
   -1 -1 -1 -1 -1 -1]; %delta energy of a particular
   class



Prob = zeros(NumClass,1);
Prob(1) = 1/(2*alph).*(1-1*tanh(beta*(2*Jx +2*Jy + B*
   muB))); %appendix E Stanley
Prob(2) = 1/(2*alph).*(1-1*tanh(beta*(2*Jx + B*muB)));
Prob(3) = 1/(2*alph).*(1-1*tanh(beta*(2*Jx - 2*Jy + B*
   muB)));
Prob(4) = 1/(2*alph).*(1-1*tanh(beta*(2*Jy + B*muB)));
Prob(5) = 1/(2*alph).*(1-1*tanh(beta*B*muB));
Prob(6) = 1/(2*alph).*(1-1*tanh(beta*(-2*Jy + B*muB)))
   ;
Prob(7) = 1/(2*alph).*(1-1*tanh(beta*(-2*Jx +2*Jy + B*
   muB)));
Prob(8) = 1/(2*alph).*(1-1*tanh(beta*(-2*Jx + B*muB)))
   ;
Prob(9) = 1/(2*alph).*(1-1*tanh(beta*(-2*Jx - 2*Jy + B
   *muB)));
Prob(10) = 1/(2*alph).*(1+1*tanh(beta*(2*Jx + 2*Jy + B
   *muB)));
Prob(11) = 1/(2*alph).*(1+1*tanh(beta*(2*Jx + B*muB)))
   ;
Prob(12) = 1/(2*alph).*(1+1*tanh(beta*(2*Jx - 2*Jy + B
   *muB)));
Prob(13) = 1/(2*alph).*(1+1*tanh(beta*(2*Jy + B*muB)))
   ;
Prob(14) = 1/(2*alph).*(1+1*tanh(beta*(B*muB)));
Prob(15) = 1/(2*alph).*(1+1*tanh(beta*(-2*Jy + B*muB))
   );
Prob(16) = 1/(2*alph).*(1+1*tanh(beta*(-2*Jx +2*Jy + B
   *muB)));
```

```
Prob(17) = 1/(2*alph).*(1+1*tanh(beta*(-2*Jx + B*muB))
   );
Prob(18) = 1/(2*alph).*(1+1*tanh(beta*(-2*Jx - 2*Jy +
   B*muB)));

% Determination of the Q coefficient
qArray(1) = nArray(1)*Prob(1); %appendix E Stanley

for i=2:NumClass
    qArray(i) = qArray(i-1) + nArray(i)*Prob(i);
end

% Determination of the class where the spin must be
   flipped
R = qArray(NumClass)*rand(1);
for k=1:NumClass
    if R<qArray(k)
        break;
    end
end
% The spin must be flipped in class k

% Calculation of energy
Energy(t+1) = Energy(t) + 2*ClassEnergy(k)/N;

%3. Determination of the spin in the class that must
   be flipped and
%change of location and class accordingly
R = floor(nArray(k)*rand(1))+1;
riga = floor(Class(k,R)/(L*18)); %row of the spin to
   flip
colonna = mod(Class(k,R)-1,L*18) + 1; %column of the
   spin to flip
locazione = Location(riga,colonna); %location of the
   spin to flip in class (k-1,R)
```

```
% Shift in last position the spin to flip


if time(t)>tempP
    tempP = tempP + NofIter; % Show every P = n*
       NofIter, n integer
    if show == 1

        figure(1)
        imagesc(mod(Location,18*18),[-1 18]);
        colormap(hot(256))

        title('Matrix LOCATION')
        set(gca,'xtick',[])
        set(gca,'ytick',[])

        figure(2)
        imagesc(Lattice);
        colormap(hot(256))
        title('Matrix LATTICE')
        set(gca,'xtick',[])
        set(gca,'ytick',[])

        figure(3);
        subplot(1,2,1)
        plot(time,Magnetization)
        hold on
        plot(time,Field(1:t))
        title('Magnetization')
        ylim([-1,1])
        hold off
        subplot(1,2,2)
        plot(time,Energy(1:t))
        hold on
        plot(time,Field(1:t))
        title('Energy')
```

```
        hold off

        figure(4)
        bar(nArray)
        ylim([0,L*L])
        title('Array N-ARRAY')

        figure(5)
        imagesc(Class.*-1+18)
        colormap(hot(256))
        title('Matrix CLASS')
        drawnow
        pause(timePause);
    end
end



% Calculation of the time required for the flip
Rparameter = qArray(18);
deltaT = -1/Rparameter*log(rand(1));

if deltaT <=P/50 % Check of whether the spin is taking
    too long to flip

% Calculation of the magnetization and time
   improvement
    Lattice(riga,colonna) = Lattice(riga,colonna)*-1;
       % Actual flipping of the spin
    Magnetization(t+1) = Magnetization(t) + 2*Lattice(
       riga,colonna)/N;
    Magnetization2(t+1) = Magnetization(t+1)^2;
    Magnetization4(t+1) = Magnetization(t+1)^4;
    time(t+1) = time(t) + deltaT;
    Field(t+1) = B;
```

```
    t = t + 1;

    lastValue = Class((mod(locazione,18*18)),nArray(
       mod(locazione,18*18))); % Last spin of the class
        that needs to shift in the position of the spin
        that is changing class
    Class((mod(locazione,18*18)),floor(locazione
       /(18*18))) = lastValue; % Substitution the last
       spin in each class in the right position
    Location(floor(lastValue/(18*L)),mod(lastValue,L
       *18)) = locazione; % Update of the varaible
       Location
    Class((mod(locazione,18*18)),nArray(mod(locazione
       ,18*18))) = 0; % Cancel of the position in class
        of the last spin that was substituted

% Update of the variables mArray and nArray
    nArray(mod(locazione,18*18)) = nArray(mod(
       locazione,18*18))-1; % nArray changes only in
       the considered class

% Determination of the new class in which the spin is
   added
    newClass = mod(mod(locazione,18*18)+8,18)+1;
    keepinmind = floor((mod(locazione,18*18)+8)/18); %
        0 if spin up, 1 if spin down
    Class(newClass,nArray(newClass)+1) = riga*18*L+
       colonna; % Substitution the last spin in class
       in the right position
    Location(riga,colonna) = newClass + 18*18*(nArray(
       newClass)+1);

% Update of nArray
   nArray(newClass) = nArray(newClass) + 1;

% Change the nearest neighbours
```

```
coordinates(1,1) = mod(riga,L) + 1;
coordinates(2,1) = colonna;
coordinates(1,2) = riga;
coordinates(2,2) = mod(colonna,L) + 1;
coordinates(1,3) = mod(riga - 2,L) + 1;
coordinates(2,3) = colonna;
coordinates(1,4) = riga;
coordinates(2,4) = mod(colonna - 2,L) + 1;

for i=1:4
    locazione = Location(coordinates(1,i),
       coordinates(2,i));
    % Shift in last position the spin to flip
    lastValue = Class((mod(locazione,18*18)),
       nArray(mod(locazione,18*18))); % Last spin
       of the class that needs to shift in the
       position of the spin that is changing class
    Class((mod(locazione,18*18)),floor(locazione
       /(18*18))) = lastValue; % Substitution the
       last spin in each class in the right
       position
    Location(floor(lastValue/(18*L)),mod(lastValue
       ,L*18)) = locazione; % Update of the
       varaible Location
    Class((mod(locazione,18*18)),nArray(mod(
       locazione,18*18))) = 0; % Cancel of the
       position in class of the last spin that was
       substituted

    % Update of the variables mArray and nArray
    nArray(mod(locazione,18*18)) = nArray(mod(
       locazione,18*18))-1; % nArray changes only
       in the considered class

    % Determination of the new class in which the
       spin is added
```

```
if keepinmind==0
    if mod(i,2)==1 % horizontal nn
        newClass = mod(mod(locazione,18*18)
           +2,18)+1; % No possibility of
           1--->10
        Class(newClass,nArray(newClass)+1) =
           coordinates(1,i)*18*L+coordinates(2,
           i);
        Location(coordinates(1,i),coordinates
           (2,i)) = newClass + 18*18*(nArray(
           newClass)+1);
        nArray(newClass) = nArray(newClass) +
           1;
    else % Vertical nn
        newClass = mod(mod(locazione,18*18)
           ,18)+1; % No possibility of 1--->10
        Class(newClass,nArray(newClass)+1) =
           coordinates(1,i)*18*L+coordinates(2,
           i);
        Location(coordinates(1,i),coordinates
           (2,i)) = newClass + 18*18*(nArray(
           newClass)+1);
        nArray(newClass) = nArray(newClass)+1;
    end
else
    if mod(i,2)==1 % Horizontal nn
        newClass = mod(mod(locazione,18*18)
           -4,18)+1; % No possibility of
           10--->1
        Class(newClass,nArray(newClass)+1) =
           coordinates(1,i)*18*L+coordinates(2,
           i);
        Location(coordinates(1,i),coordinates
           (2,i)) = newClass + 18*18*(nArray(
           newClass)+1);
        nArray(newClass) = nArray(newClass) +
```

```
                    1;
                else % Vertical nn
                    newClass = mod(mod(locazione,18*18)
                    -2,18)+1; % No possibility of
                    1--->10
                    Class(newClass,nArray(newClass)+1) =
                    coordinates(1,i)*18*L+coordinates(2,
                    i);
                    Location(coordinates(1,i),coordinates
                    (2,i)) = newClass + 18*18*(nArray(
                    newClass)+1);
                    nArray(newClass) = nArray(newClass) +
                    1;
                end
            end
        end
    else % No flipping is performed, the system time is
        incremented by P/50
            Magnetization(t+1) = Magnetization(t); % First
            -order magnetization
            Magnetization2(t+1) = Magnetization(t+1)^2; %
            Second-order magnetization (Useful to
            compute Chi)
            Magnetization4(t+1) = Magnetization(t+1)^4; %
            Fourth-order magnetization (Useful to
            compute Binder Cumulant)
            time(t+1) = time(t) + P/50;
            Field(t+1) = B;
            t = t + 1;
        end
    end
end
```